Characterization of a Feline Influenza A(H7N2) Virus

Masato Hatta,[1] Gongxun Zhong,[1] Yuwei Gao,[1] Noriko Nakajima,[1] Shufang Fan,[1] Shiho Chiba, Kathleen M. Deering, Mutsumi Ito, Masaki Imai, Maki Kiso, Sumiho Nakatsu, Tiago J. Lopes, Andrew J. Thompson, Ryan McBride, David L. Suarez, Catherine A. Macken, Shigeo Sugita, Gabriele Neumann, Hideki Hasegawa, James C. Paulson, Kathy L. Toohey-Kurth, Yoshihiro Kawaoka

During December 2016–February 2017, influenza A viruses of the H7N2 subtype infected ≈500 cats in animal shelters in New York, NY, USA, indicating virus transmission among cats. A veterinarian who treated the animals also became infected with feline influenza A(H7N2) virus and experienced respiratory symptoms. To understand the pathogenicity and transmissibility of these feline H7N2 viruses in mammals, we characterized them in vitro and in vivo. Feline H7N2 subtype viruses replicated in the respiratory organs of mice, ferrets, and cats without causing severe lesions. Direct contact transmission of feline H7N2 subtype viruses was detected in ferrets and cats; in cats, exposed animals were also infected via respiratory droplet transmission. These results suggest that the feline H7N2 subtype viruses could spread among cats and also infect humans. Outbreaks of the feline H7N2 viruses could, therefore, pose a risk to public health.

Influenza A viruses are endemic in humans and enzootic in other mammalian species including swine and horses; occasional infections of other mammalian species including whales, seals, sea lions, felidae in zoos, and other species have been reported (*1*). Reports of influenza A virus infections in dogs and cats were rare until 2004, when equine influenza viruses of the H3N8 subtype caused outbreaks in greyhounds in Florida (*2*). Since then, influenza viruses of the H3N8 and H3N2 subtypes have caused several outbreaks in dogs in the United States and South Korea (*3*–*5*).

Author affiliations: University of Wisconsin–Madison, Madison, Wisconsin, USA (M. Hatta, G. Zhong, Y. Gao, S. Fan, S. Chiba, K.M. Deering, T.J. Lopes, G. Neumann, K.L. Toohey-Kurth, Y. Kawaoka); National Institute of Infectious Diseases, Tokyo, Japan (N. Nakajima, H. Hasegawa); University of Tokyo, Tokyo (M. Ito, M. Imai, M. Kiso, S. Nakatsu, Y. Kawaoka); The Scripps Research Institute, La Jolla, California, USA (A.J. Thompson, R. McBride, J.C. Paulson); US Department of Agriculture, Athens, Georgia, USA (D.L. Suarez); The University of Auckland, Auckland, New Zealand (C. A. Macken); Japan Racing Association, Tochigi, Japan (S. Sugita)

DOI: https://doi.org/10.3201/eid2401.171240

Until recently, only 1 major influenza A virus outbreak had been reported in cats (*6*). This changed in December 2016 with the outbreak of low pathogenic avian influenza A viruses of the H7N2 subtype in animal shelters in New York. Approximately 500 cats were infected in December 2016–February 2017; most of which experienced a mild illness with coughing, sneezing, and runny nose from which they recovered fully. Severe pneumonia developed in 1 elderly animal with underlying health issues, which was euthanized. A veterinarian who had treated an infected animal also became infected with the feline influenza A(H7N2) virus and experienced a mild, transient illness, suggesting the potential for these viruses to infect humans. While this manuscript was being prepared, Belser et al. reported that the H7N2 subtype virus isolated from the human case caused a mild disease in mice and ferrets, but was not transmitted among ferrets (*7*). We assessed feline H7N2 subtype viruses isolated from infected cats during the outbreak for their replicative ability, pathogenicity, and transmissibility in mammals; in contrast to the findings recently published by Belser et al. (*7*), we detected productive infection of co-housed ferrets, although with low efficiency. We also conducted extensive pathology and transmission studies in cats, and detected feline virus transmission via respiratory droplets to exposed cats. Our study provides additional data on the risk that the feline H7N2 subtype viruses pose to public health.

Methods

Cells and Viruses

The origins and growth conditions of all cell lines used in this study are described in the online Technical Appendix (https://wwwnc.cdc.gov/EID/article/24/1/17-1240-Techapp1.pdf). The feline H7N2 subtype viruses used in this study were isolated from swabs collected from cats with influenza-like symptoms during the outbreak in an animal shelter in New York in December 2016. We obtained A/chicken/New York/22409–4/1999 (H7N2, A/chicken/

[1]These authors contributed equally to this article.

NY/99) virus from the Agricultural Research Service, US Department of Agriculture (*8*). We deposited the viral gene sequences obtained in this study to GenBank. We amplified the feline virus in Madin-Darby canine kidney (MDCK) cells and the A/chicken/NY/99 virus in 10-day-old embryonated chicken eggs.

Growth Kinetics of Viruses in Cell Culture

We infected cells with viruses at a 0.005 multiplicity of infection, incubated them for 1 hour at 37°C, washed twice, and cultured with 1× minimal essential medium containing 0.3% bovine serum albumin and trypsin treated with L-1-tosylamide-2-phenylethyl chloromethyl ketone at 33°C and 37°C (37°C and 39°C for chicken embryo fibroblast cells) for various periods. We determined virus titers at the indicated time points by use of plaque assays in MDCK cells. The statistical analyses are described in the online Technical Appendix.

Infection of Animals

To determine the pathogenicity of the viruses in infected mice, we anesthetized three 6-week-old female BALB/c mice (Jackson Laboratory, Bar Harbor, ME, USA) for each virus with isoflurane and inoculated intranasally with 10-fold serially diluted virus in a 50-μL volume. The mice were monitored daily for 14 days and checked for changes in body weight and morbidity and mortality. We euthanized animals if they lost more than 25% of their initial bodyweight.

To determine the pathogenicity of the viruses in infected ferrets and cats, we inoculated 6-month-old female ferrets (Triple F Farms, Sayre, PA, USA; 3 per group; serologically negative by hemagglutination inhibition assay for currently circulating human influenza viruses), and unvaccinated 4- to 5-month-old female specific-pathogen-free cats (Liberty Research, Waverly, NY, USA; 3 per group) intranasally with 10^6 PFU of viruses in 0.5 ml of phosphate-buffered saline. We monitored the animals daily for changes in bodyweight, body temperature, and clinical signs for 14 days.

For virus replication in organs and pathology analyses, we worked with groups of mice (12 per group), ferrets (6 per group), and cats (6 per group).We inoculated the animals intranasally with 10^5 PFU (mice) in 0.05 ml of phosphate-buffered saline or 10^6 PFU (ferrets and cats) of viruses in 0.5 ml of phosphate-buffered saline. On days 3 and 6 postinfection, we euthanized 6 mice, 3 ferrets, and 3 cats in each group for pathological analysis and virus titration in organs (by use of plaque assays in MDCK cells).

Virus Transmission Studies in Ferrets and Cats

For direct contact transmission experiments, we housed 3 ferrets per group in regular ferret cages and 3 cats per group in large dog transporter cages (online Technical Appendix Figure 1), and infected them intranasally with 10^6 PFU (500 μL) of viruses. One day later, we housed 1 virus-naive animal with each infected animal. We collected nasal washes from the infected ferrets and nasal swabs from the infected cats on day 1 after infection, and from the exposed animals on day 1 after exposure and then every other day (for up to 11 days). We determined virus titers in the nasal washes and swabs by performing plaque assays in MDCK cells. We monitored all animals daily for disease symptoms and changes in bodyweight and temperature for 14 days.

We performed airborne transmission experiments by using ferret isolators (Showa Science, Tokyo, Japan) (*9*–*11*) or regular cat cages. In these settings, there was no directional airflow from the infected to the exposed animals. We inoculated 3 animals per group intranasally with 10^6 PFU (500 μL) of viruses. One day after infection, we placed 3 immunologically naive animals (exposed animals) each in a cage adjacent to an infected animal. This setting prevented direct and indirect contact between animals but allowed spread of influenza virus by respiratory droplet. We spaced the ferret cages 5 cm apart and the cat cages 35 cm apart. We monitored the animals and assessed virus titers as described above.

Results

Genetic and Phylogenetic Analysis of Feline Influenza(H7N2) Viruses Isolated in Animal Shelters in New York, December 2016

We obtained swabs (collected on the same day) from 5 cats that experienced influenza-like symptoms during the outbreak at an animal shelter in New York, NY, in December 2016. After inoculation of these samples into MDCK cells, we isolated 5 pleomorphic influenza A viruses of the H7N2 subtype (Table 1; online Technical Appendix Figure 2). The HA consensus sequences of the 5 isolates (established by Sanger sequence analysis) displayed >99.9% similarity at the nucleotide level (Table 1). Phylogenetic analyses demonstrated that the 8 viral RNA segments of the 5 feline H7N2 viruses are most closely related to poultry influenza A(H7N2) viruses detected in the New York area in the late 1990s through early 2000s (Figure 1; online Technical Appendix Figures 3–9), suggesting that the 2016 feline H7N2 virus isolates descended from viruses that circulated more than a decade ago in the northeastern United States.

The HA protein of the 2016 feline H7N2 subtype virus encodes a single arginine residue at the hemagglutinin cleavage site (PEKPKPR↓G; the arrow indicates the cleavage site that creates the HA1 and HA2 subunits), indicative of low pathogenicity in chickens. Antigenically, A/feline/New York/WVDL-14/2016 (A/feline/NY/16) differs from other, closely related H7 viruses (online Technical Appendix Table 1); for example, its HA deviates by 27 aa from the closely related A/chicken/NY/22409–4/1999 HA. The

Table 1. Amino acid differences among feline influenza A(H7N2) virus isolates, New York, NY, USA*

	Amino acid positions in the viral proteins					
	PB2	PB1-F2	PA	NA		NS2
Virus	448	42	57	40	62	74
A/feline/New York/WVDL-3/2016	**S**	**C**	**Q**	**Y**	**C**	D
A/feline/New York/WVDL-9/2016	N	Y	R	H	**C**	**E**
A/feline/New York/WVDL-14/2016	**S**	**C**	**Q**	**Y**	**C**	**E**
A/feline/New York/WVDL-16/2016	**S**	**C**	**Q**	**Y**	F	**E**
A/feline/New York/WVDL-20/2016	**S**	**C**	**Q**	**Y**	**C**	D

*Consensus sequences among the 5 H7N2 subtype viruses are shown in bold. Amino acids: C, cysteine; D, aspartic acid; E, glutamic acid; F, phenylalanine; H, histidine; L, leucine; N, asparagine; Q, glutamine; R, arginine; S, serine; Y, tyrosine. Viral proteins: NA, neuraminidase; NS, nonstructural protein; PA, polymerase acidic; PB, polymerase basic.

neuraminidase (NA) and ion channel (M2) proteins of the H7N2 viruses do not encode amino acids that confer resistance to neuraminidase or ion channel inhibitors. Inspection of the remaining feline H7N2 viral proteins revealed an absence of the most prominent amino acid changes known to facilitate adaptation to mammals, such as PB2–627K (*16*). These data thus suggest the 2016 feline H7N2 subtype viruses are avian-derived influenza viruses of low pathogenicity in avian and mammalian species.

Replication of Feline and Avian H7N2 Subtype Viruses in Cultured Cells

To characterize the replicative ability of the 2016 feline H7N2 viruses in cultured cells, we compared A/feline/NY/16 (which encodes the consensus amino acid sequence of the 5 isolates) with a closely related 1999 avian influenza virus, A/chicken/NY/22409–4/1999 (H7N2, A/chicken/NY/99) (Figure 1; online Technical Appendix Figures 3–9), which was isolated from a chicken in a live-bird market in New York state in 1999 (*8*). There are a total of 97 aa differences between A/feline/NY/16 and A/chicken/NY/99 viruses (12 aa differences in polymerase basic 2 (PB2), 7 in polymerase basic 1 (PB1), 12 in polymerase acidic (PA), 27 in hemagglutinin (HA), 8 in nucleoprotein (NP), 11 in neuraminidase (NA), 7 in matrix protein 1 (M1), 4 in matrix protein 2 (M2), and 9 in nonstructural protein 1 (NS1). Canine, human, feline, and chicken cells were infected at a multiplicity of infection of 0.005 at temperatures mimicking those of the upper and lower respiratory tract of the respective species (i.e., 37°C and 39°C for chicken cells; 33°C and 37°C for the remaining cells) (Figure 2). In canine MDCK, feline Clone81, and human Calu-3 cells, A/feline/NY/16 replicated at least as efficiently as A/chicken/NY/99 virus, while both viruses replicated to low titers in human A549 cells. Of note, A/feline/NY/16 virus replicated less efficiently than A/chicken/NY/99 virus in feline lung Fc2Lu cells. In chicken embryo fibroblast cells, A/feline/NY/16 virus replicated more slowly than A/chicken/NY/99 virus at early time points and reached its highest titers at later time points. When we compared virus growth at the 2 temperatures tested (i.e., 37°C and 39°C for chicken cells; 33°C and 37°C for the remaining cells), we observed similar trends (for example, in MDCK cells, A/feline/NY/16 replicated more efficiently than A/chicken/NY/99 at both temperatures tested).

Replication and Pathogenicity of Feline and Avian H7N2 Subtype Viruses in Mice

To assess the replication of A/feline/NY/16 and A/chicken/NY/99 viruses in mice, 3 mice per group were inoculated intranasally with 10-fold dilutions of viruses, and their bodyweight and morbidity and mortality were monitored daily for 14 days. Mice infected with A/feline/NY/16 virus did not experience weight loss or signs of disease, whereas infection with 10^6 PFU of A/chicken/NY/99 virus caused severe weight loss and required euthanasia (online Technical Appendix Figure 10).

A/feline/NY/16 replicated efficiently in the nasal turbinates and less efficiently in the lungs of infected animals (online Technical Appendix Figure 11); no virus was isolated from the other organs tested (i.e., brains, kidneys, livers, and spleens; data not shown). A/chicken/NY/99 replicated more efficiently in the lungs than in the nasal turbinates, consistent with immunohistochemistry analyses that detected A/feline/NY/16 virus antigens mainly in the upper respiratory organs of infected mice, whereas A/chicken/NY/99 virus antigens were detected more frequently in the lower respiratory organs (online Technical Appendix Figure 12).

Replication and Pathogenicity of Feline and Avian H7N2 Subtype Viruses in Ferrets

Ferrets intranasally infected with 10^6 PFU of A/feline/NY/16 or A/chicken/NY/99 virus did not lose bodyweight (online Technical Appendix Figure 13) but 2 of the ferrets infected with A/chicken/NY/99 virus had high fevers on day 1 postinfection. Both viruses replicated efficiently in the nasal turbinates and were also isolated from the trachea and lungs of some animals (Table 2), consistent with similar antigen distributions for both viruses (online Technical Appendix Figure 14). No viruses were isolated from any of the other organs tested.

Replication and Pathogenicity of Feline and Avian H7N2 Subtype Viruses in Cats

The infection of ≈500 cats with H7N2 subtype viruses in animal shelters in New York in December 2016 suggested

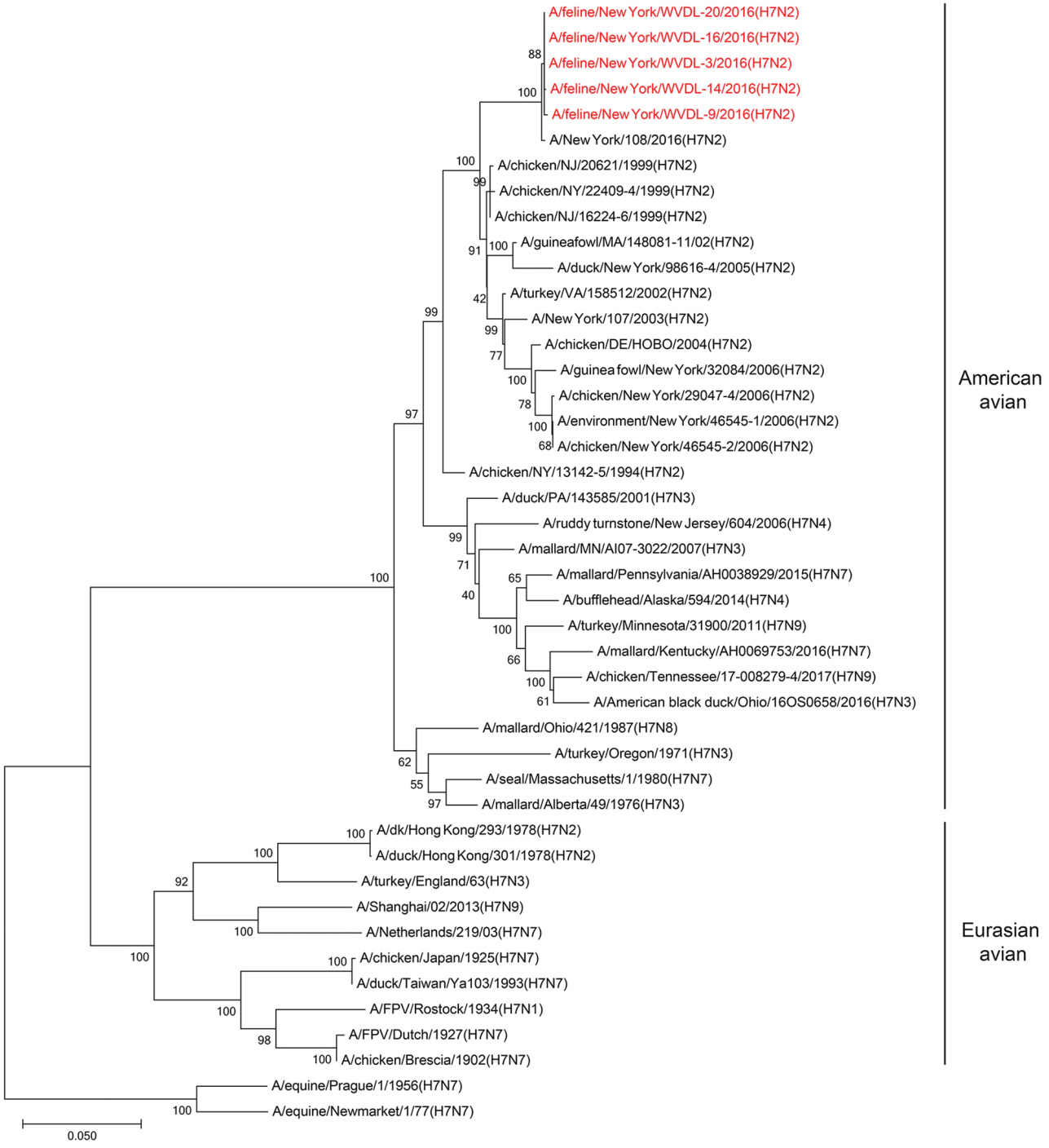

Figure 1. Phylogenetic tree of influenza A viral hemagglutin segments from New York, NY, USA, compared with reference viruses. Phylogenetic analysis was performed for selected influenza A viruses representing major lineages. The evolutionary history was inferred using the neighbor-joining method (*12*). The optimal tree with the branch length sum of 1.22521320 is shown. The percentage of replicate trees in which the associated taxa clustered together in the bootstrap test (500 replicates) is shown next to the branches (*13*). The tree is drawn to scale, with branch lengths in the same units as those of the evolutionary distances used to infer the phylogenetic tree. The evolutionary distances were computed using the Tamura 3-parameter method (*14*) and are in the units of the number of base substitutions per site. The analysis involved 44 nt sequences. Codon positions included were 1st + 2nd + 3rd + noncoding. All positions containing gaps and missing data were eliminated. The final dataset contained a total of 1,612 positions. Evolutionary analyses were conducted in MEGA7 (*15*).

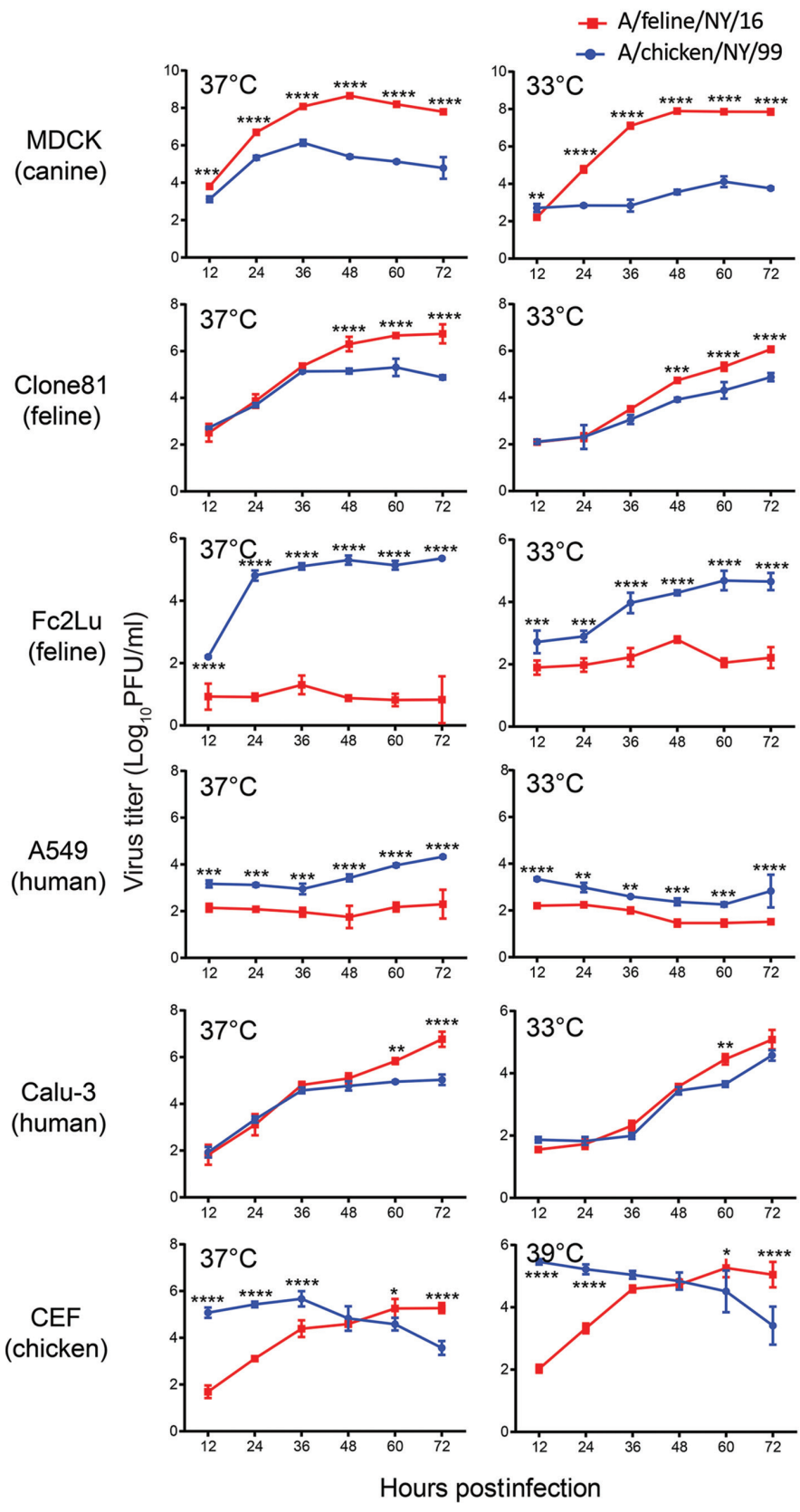

Figure 2. Growth properties of A/feline/NY/16 and A/chicken/NY/99 influenza A(H7N2) viruses in mammalian and avian cells at different temperatures, New York, NY, USA. Cells were infected with viruses at a multiplicity of infection of 0.005 and incubated at 33°C and 37°C (or at 37°C and 39°C for avian CEF cells). Supernatants were harvested at the indicated time points. Virus titers were determined by use of plaque assays in Madin-Darby canine kidney (MDCK) cells. The species from which the cell lines are derived are shown. The values presented are the averages of 3 independent experiments ±SD. Statistical significance was determined as described in the online Technical Appendix (https://wwwnc.cdc.gov/EID/article/24/1/17-1240-Techapp1.pdf). *p≤0.05; **p≤0.01; ***p≤0.001; ****p≤0.0001. A549, human lung carcinoma epithelial cells; Clone81, cat kidney fibroblast cells; Fc2Lu, cat lung cells; CEF, chicken embryo fibroblast cells.

Table 2. Virus titers in organs of ferrets and cats infected with A/feline/NY/16 or A/chicken/NY/99 influenza A(H7N2) viruses, New York, NY, USA*

Species and virus	Days postinfection	Animal ID no.	Virus titers in organs of infected animals, log_{10} PFU/g					
			Nasal turbinates	Trachea	Lung	Small intestine	Colon	Other organs†
Ferret								
A/feline/NY/16	3	1	4.4	3.3	4.7	–	–	–
		2	5.2	–	2.4	–	–	–
		3	5.4	–	–	–	–	–
	6	4	3.1	–	–	–	–	–
		5	5.8	–	–	–	–	–
		6	6.0	–	–	–	–	–
A/chicken/NY/99	3	7	5.9	3.3	–	–	–	–
		8	6.0	–	–	–	–	–
		9	6.6	3.4	–	–	–	–
	6	10	4.2	–	–	–	–	–
		11	4.5	–	5.7	–	–	–
		12	4.4	–	–	–	–	–
Cat								
A/feline/NY/16	3	1	3.9	4.8	–	–	–	–
		2	4.1	6.6	5.8	–	–	–
		3	6.9	7.0	5.8	–	–	–
	6	4	6.3	6.2	6.1	–	2.3	–
		5	7.7	7.8	4.7	–	–	–
		6	5.9	6.2	6.7	3.8	–	–
A/chicken/NY/99	3	7	6.4	5.8	3.9	–	–	–
		8	2.0	–	–	–	–	–
		9	6.1	–	–	4.9	–	–
	6	10	6.4	–	5.0	–	–	–
		11	4.6	–	–	–	–	–
		12	6.7	4.0	–	–	–	–

*–, no virus detected.
†Brain, spleen, kidneys, liver, and pancreas.

efficient replication of these viruses in felines. However, it was unclear whether these viruses were restricted to the respiratory organs or caused systemic infection. Cats intranasally infected with 10^6 PFU of A/feline/NY/16 or A/chicken/NY/99 did not lose bodyweight (Figure 3); however, fever was detected in 1 animal infected with A/feline/NY/16, and 1 infected with A/chicken/NY/99 virus; and a different animal infected with A/feline/NY/16 sneezed intensely on day 3 postinfection, but recovered fully.

A/feline/NY/16 virus replicated efficiently in the nasal turbinates, trachea, and lungs of infected cats (with the exception of 1 cat with a virus-negative lung sample on day 3 postinfection; Table 2). We isolated A/chicken/NY/99 virus mostly from nasal turbinates, with limited replication in the trachea and lung. These findings are consistent with the detection of A/feline/NY/16 antigen in both the upper and lower respiratory organs of infected cats, whereas A/chicken/NY/99 antigen was detected mainly in the nasal turbinates (Figure 4). A/feline/NY/16 and A/chicken/NY/99 viruses were also isolated from the jejunum or colon of some of the infected animals (Table 2), although viral antigen was not detected in the intestines of cats infected with A/chicken/NY/99 or A/feline/NY/16 virus. These results demonstrate that the feline H7N2 virus replicates efficiently in the upper and lower respiratory tract of cats, reflecting adaptation of the virus to its new host.

All cats infected with the A/feline/NY/16 virus exhibited histologic lesions in their nasal turbinates, tracheas, and lungs. Nasal turbinate pathology was moderate to severe in 5 of 6 cats with multifocal to diffuse distribution of lesions (Figure 5, panel A). The tracheas of these cats exhibited mild to moderate histopathology (Figure 5, panel B), whereas the lungs exhibited multifocal to coalescing histopathology centered mostly on the bronchioles, with 3 of 6 cats possessing moderately severe lesions (Figure 5, panel C). Similar histopathological changes were found in cats infected with A/chicken/NY/99 virus. Appreciable histopathology was also noted in the small intestine (duodenum) of cats infected with A/feline/NY/16 and A/chicken/NY/99 viruses (Figure 5, panel D; cat ID nos. 1, 2, 4, 8, 10, and 12 in Table 2), although virus was detected in the intestines of only 3 cats (cat ID nos. 4, 6, and 9 in Table 2). The correlation between virus replication and histologic lesions in cat intestines is currently unknown.

Transmission of Feline and Avian H7N2 Subtype Viruses in Ferrets and Cats

The fulminant spread of the feline H7N2 subtype viruses among cats, and the confirmed H7N2 virus infection of a veterinarian who treated the animals, indicate that these originally avian influenza viruses have the ability to transmit among mammals. To test the transmissibility of feline and

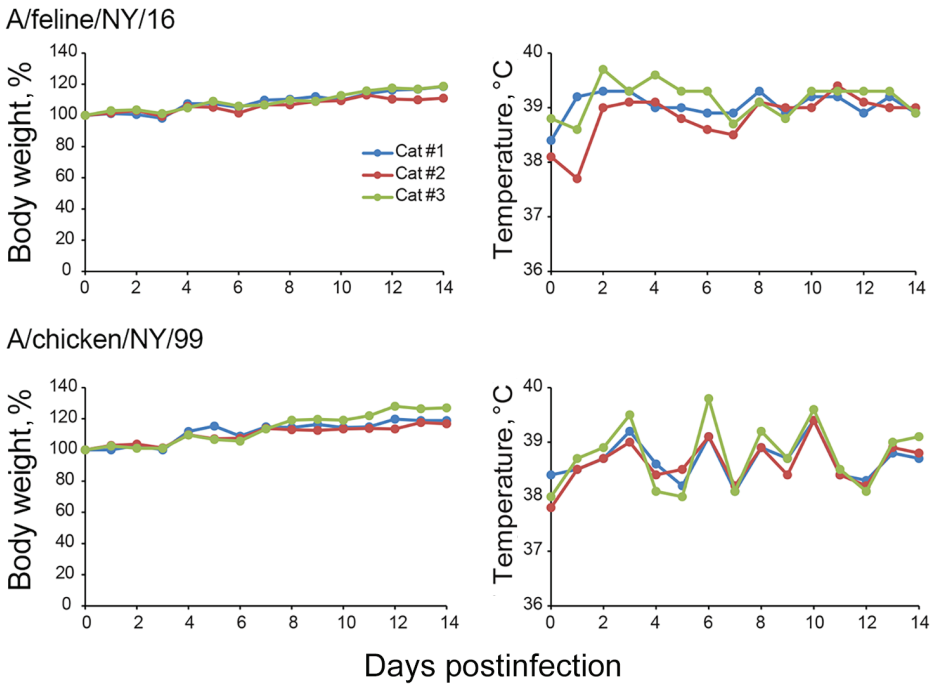

Figure 3. Body weight and temperature changes in cats infected with A/feline/NY/16 and A/chicken/NY/99 influenza A(H7N2) viruses, New York, NY, USA. Three cats per group were infected intranasally with 10^6 PFU of viruses and monitored for bodyweight and temperature changes.

avian H7N2 subtype viruses in ferrets, 3 animals per group (each placed in a separate cage) were infected intranasally with 10^6 PFU (500 μL) of A/feline/NY/16 or A/chicken/NY/99 virus. One day later, we housed 1 naive ferret with each of the infected ferrets (direct contact transmission experiment), or placed naive ferrets in wireframe cages (within

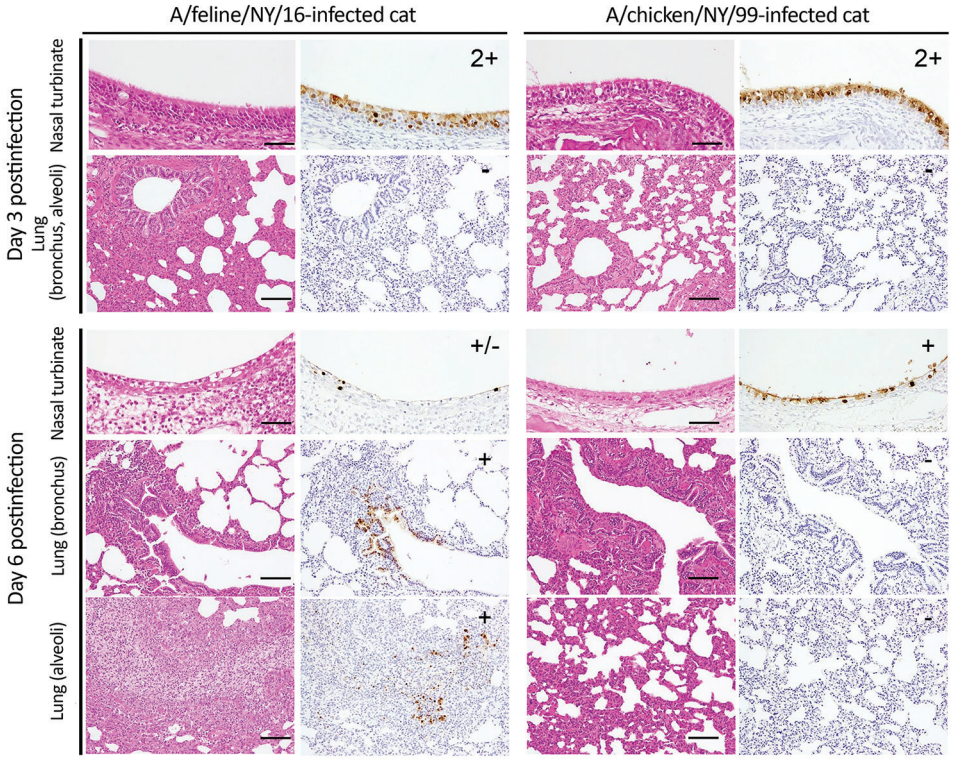

Figure 4. Immunohistochemistry findings in cats infected with influenza A(H7N2) virus, New York, NY, USA. Shown are representative sections of nasal turbinates and lungs of cats infected with the indicated viruses on days 3 and 6 postinfection. Three cats per group were infected intranasally with 10^6 PFU of virus, and tissues were collected on days 3 and 6 postinfection. Type A influenza virus nucleoprotein (NP) was detected by a mouse monoclonal antibody to this protein. For nasal turbinate sections: –, no NP-positive cells; +/–, NP-positive cells detected in 1–2 focal regions; +, NP-positive cells detected in >2 focal regions; 2+, NP-positive cells in large regions. For bronchus and alveolar sections: –, no NP-positive cells; +/–, ≥5 NP-positive cells; +, ≥6 NP-positive cells. NP-positive cells were detected in focal, but not in diffuse bronchial and alveolar sections. For all analyses, the entire sections were evaluated. Scale bars indicate 50 μm (nasal turbinates) or 100 μm (lung).

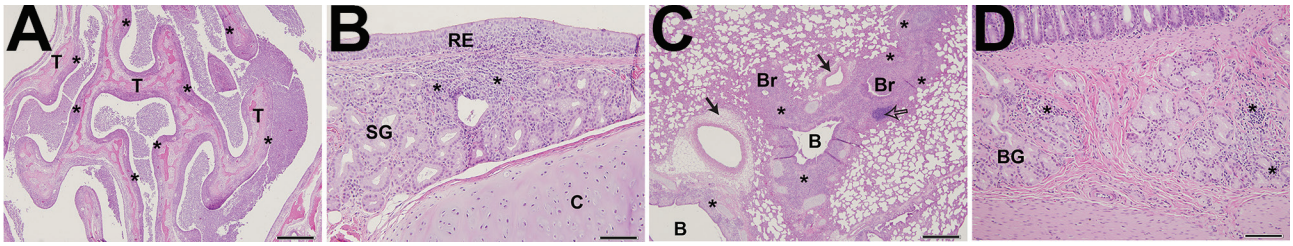

Figure 5. Pathology findings in cats infected with A/feline/NY/16 influenza A(H7N2) virus on day 6 postinfection, New York, NY, USA. A) In lungs, moderately severe histopathologic changes are present in the lower airways. The lamina propria of bronchi (B) and bronchioles (Br) and the surrounding interstitium are infiltrated by numerous histiocytes, lymphocytes, and plasma cells (*), which also extend into and expand neighboring alveolar septa. The infiltrates extend into and expand nearby alveolar septa. The lumina of bronchioles are filled with numerous foamy macrophages, viable and degenerating neutrophils, proteinaceous fluid, and sloughed respiratory epithelial cells. Hyperplasia of bronchiole-associated lymphoid tissue (open arrow) and perivascular edema (solid arrow) are present. Scale bar indicates 500 µm. B) In nasal cavities, copious amounts of exudate are present comprising numerous degenerating and necrotic neutrophils, cellular debris, proteinaceous fluid, and strands of mucin. The respiratory epithelium covering the nasal turbinates (T) is extensively eroded. The underlying lamina propria appears diffusely bluish-purple due to infiltration by moderate-to-large numbers of histiocytes, neutrophils, lymphocytes, and plasma cells (*). Scale bar indicates 500 µm. C) In the trachea, a locally extensive focus of inflammation is present in the tracheal wall. Moderate numbers of histiocytes, lymphocytes, and plasma cells, and a few neutrophils, infiltrate the respiratory epithelium (RE), lamina propria, and submucosa. Submucosal glands (SG) are surrounded by the inflammatory infiltrates and effaced in the areas of heaviest infiltration (*). Tracheal cartilage (C). Scale bar indicates 100 µm. D) In the duodenum, inflammatory cell infiltrates (*) in the submucosa of the duodenum are present between and around Brunner's glands (BG). Scale bar indicates 100 µm.

transmission isolators) ≈5 cm from the cages containing the infected ferrets as a respiratory droplet transmission experiment. We collected nasal wash samples from infected, contact, and exposed animals on day 1 after infection, contact, or exposure, and then every other day; we determined virus titers in nasal wash samples by use of plaque assays in MDCK cells (Table 3). In respiratory droplet transmission experiments, ferrets infected with A/feline/NY/16 or A/chicken/NY/99 virus secreted virus, but exposed animals were virus negative and did not seroconvert (Table 3). Among the direct contact animals, we detected virus in 1 ferret from the A/feline/NY/16-inoculated group and 2 from the A/chicken/NY/99-inoculated group; these 3 animals seroconverted, although the HI titer of 1 of the animals was low.

Table 3. Influenza A(H7N2) virus titers in nasal wash samples from ferret transmission studies, New York, NY, USA*

Virus and transmission mode	Pair	Action	Virus titers in nasal wash samples by days after infection, exposure, or contact, log_{10} PFU/mL						Seroconversion, HI titer†
			1	3	5	7	9	11	
A/feline/NY/16									
Respiratory droplets	1	Infection	4.2	5.6	5.0	–	–	–	320
		Exposure	–	–	–	–	–	–	<10
	2	Infection	4.6	4.3	5.4	–	–	–	320
		Exposure	–	–	–	–	–	–	<10
	3	Infection	5.3	5.0	4.8	2.8	–	–	640
		Exposure	–	–	–	–	–	–	<10
Direct contact	1	Infection	3.6	4.1	5.0	2.0	–	–	640
		Contact	–	–	–	–	–	–	<10
	2	Infection	5.5	5.1	4.3	1.3	–	–	320
		Contact	–	–	–	–	–	–	<10
	3	Infection	5.0	5.2	5.2	2.9	–	–	640
		Contact	–	–	4.2	5.3	4.6	–	320
A/chicken/NY/99									
Respiratory droplets	1	Infection	5.8	4.0	4.3	–	–	–	160
		Exposure	–	–	–	–	–	–	<10
	2	Infection	5.6	4.2	3.5	–	–	–	160
		Exposure	–	–	–	–	–	–	<10
	3	Infection	5.1	3.7	3.5	–	–	–	320
		Exposure	–	–	–	–	–	–	<10
Direct contact	1	Infection	4.3	4.3	3.0	–	–	–	160
		Contact	–	–	3.8	4.3	3.4	–	160
	2	Infection	4.2	3.8	3.8	–	–	–	160
		Contact	–	–	2.1	–	–	–	10
	3	Infection	4.9	3.9	4.3	–	–	–	320
		Contact	–	–	–	–	–	–	10

*HI, hemagglutination inhibition; –, no virus detected.
†Serum specimens were collected on day 18 after infection, exposure, or contact, and examined using an HI assay. The HI titer is the inverse of the highest dilution of serum that completely inhibited hemagglutination.

Table 4. Influenza A(H7N2) virus titers in nasal swab samples from cat transmission studies, New York, NY, USA*

Virus and transmission mode	Pair	Action	Virus titers in nasal swab samples by days after infection, exposure, or contact, log_{10} PFU/mL							Seroconversion, HI titer†
			1	3	5	7	9	11	13	
A/feline/NY/16										
Respiratory droplets	1	Infection	5.6	4.7	4.3	3.0	–	–	–	320
		Exposure	–	–	–	–	5.2	–	–	160
	2	Infection	4.5	2.7	5.0	4.6	–	–	–	320
		Exposure	–	–	–	–	–	5.4	–	80
	3	Infection	4.8	3.2	5.3	3.6	–	–	–	320
		Exposure	–	–	–	–	–	–	–	<10
Direct contact	1	Infection	5.9	4.6	3.4	–	–	–	–	320
		Contact	–	–	2.0	5.4	–	–	–	320
	2	Infection	6.0	5.0	4.6	–	–	–	–	640
		Contact	–	–	–	–	–	–	–	80
	3	Infection	4.9	4.9	4.4	4.2	–	–	–	640
		Contact	–	5.2	5.4	5.2	–	–	–	160
A/chicken/NY/99										
Respiratory droplets	1	Infection	4.0	3.7	4.7	–	–	–	–	320
		Exposure	–	–	–	–	–	–	–	20
	2	Infection	–	–	–	–	–	–	–	320
		Exposure	–	–	–	–	–	–	–	20
	3	Infection	2.6	1.6	2.3	–	–	–	–	80
		Exposure	–	–	–	–	–	–	–	160
Direct contact	1	Infection	4.5	2.4	4.5	–	–	–	–	80
		Contact	–	–	–	–	–	–	–	160
	2	Infection	3.4	4.8	4.1	3.6	–	–	–	160
		Contact	–	–	–	–	–	–	–	40
	3	Infection	3.4	3.5	3.2	3.3	–	–	–	160
		Contact	–	–	–	–	–	–	–	20

*HI, hemagglutination inhibition; –, no virus detected.
†Serum samples were collected on day 18 after infection, exposure, or contact, and examined by use of an HI assay. The HI titer is the inverse of the highest dilution of serum that completely inhibited hemagglutination.

We conducted the transmission study in cats in the same way as the study in ferrets; we spaced cages 35 cm apart to prevent direct contact between the inoculated and exposed animals (online Technical Appendix Figure 1, panel A). All infected cats secreted viruses for 5–7 days after infection and seroconverted, except for 1 cat infected with A/chicken/NY/99 virus, which seroconverted but did not shed virus (Table 4). We did not isolate A/chicken/NY/99 virus from contact or exposed animals, although these animals seroconverted (Table 4). Direct contact transmission of A/feline/NY/16 virus was detected in all 3 pairs of cats, with both seroconversion and virus isolation in 2 pairs (Table 4). Respiratory droplet transmission of A/feline/NY/16 occurred in 2 pairs of animals, with high virus titers detected in the nasal secretions of the exposed animals on days 9 and 11 postexposure, respectively; both of the exposed animals also seroconverted (Table 4). In the third transmission pair, the exposed animal did not shed virus or seroconvert. Taken together, we demonstrated that A/feline/NY/16 virus has the ability to transmit among cats via contact and respiratory droplets; the relative contribution of these modes of transmission to the H7N2 subtype virus outbreaks in cat shelters in New York is unknown.

Receptor-Binding Specificity of Feline and Avian H7N2 Subtype Viruses

Avian influenza viruses isolated from their natural reservoir (i.e., wild aquatic birds) are often restricted in their ability to infect mammalian cells because of their preferential binding to α2,3-linked sialic acids, whereas most human influenza viruses preferentially bind to α2,6-linked sialic acids (*17–19*). We performed glycan array analysis with A/feline/NY/16, A/chicken/NY/99, and Kawasaki/173-PR8, a control virus possessing the HA and NA genes of the seasonal human A/Kawasaki/173/2001 (H1N1) virus and the remaining genes from A/PR/8/34 (H1N1) virus. As expected, Kawasaki/173-PR8 virus bound to α2,6-linked sialosides (Figure 6; online Technical Appendix Table 2). A/chicken/NY/99 virus bound to both α2,6- and α2,3-linked sialosides, consistent with the dual avian/human receptor-binding specificity of influenza viruses isolated from land-based poultry (*1*). Of note, A/feline/NY/16 virus bound strongly to α2,3-linked sialosides (i.e., avian-type receptors) with negligible binding to human-type receptors.

Next, we examined the prevalence of α2,3- and α2,6-linked sialosides in the feline airway and intestines of an immunologically naive cat by using lectins that detect α2,3-linked (i.e., MAA I and MAA II) and α2,6-linked sialosides (i.e., SNAI). MAA I and MAIA II bound to epithelial cells throughout the feline airway, whereas SNA binding was detected only in the trachea and bronchus (Figure 7), consistent with the findings of other research groups (*20–22*). We did not detect sialosides in the cat intestine. The predominance of avian-type receptors in

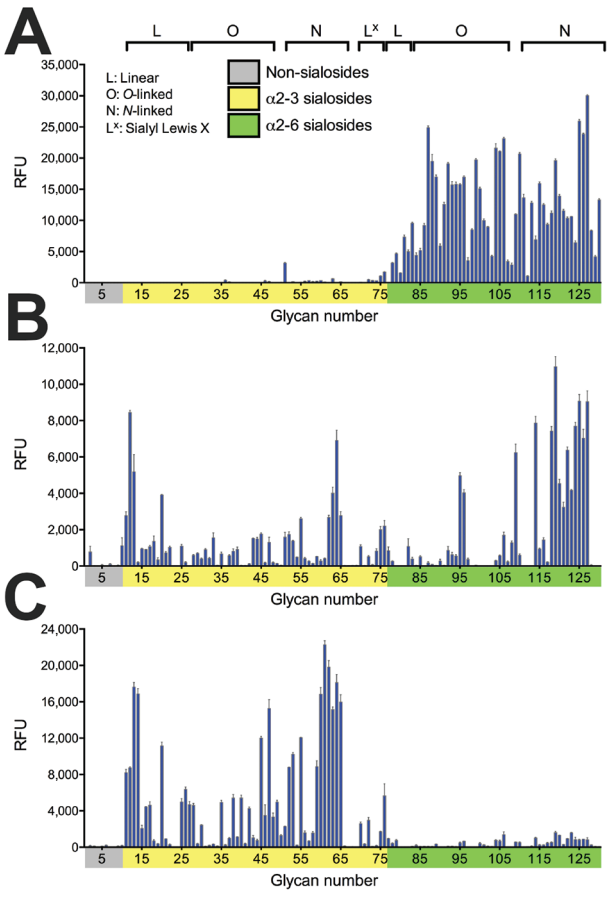

Figure 6. Receptor-binding specificities of influenza A viruses, New York, NY, USA. A) A representative human virus, A/Kawasaki/173-PR8(H1N1) is shown for comparison with B) the avian influenza A(H7N2) virus A/chicken/NY/99 and C) the feline influenza A(H7N2) virus A/feline/NY/16. Receptor-binding specificities of the avian and feline viruses were compared with those of the human virus in a glycan microarray containing α2,3- and α2,6-linked sialosides. Error bars represent SDs calculated from 4 replicate spots of each glycan. RFU, relative fluorescence units. A complete list of the glycans used is shown in online Technical Appendix Table 2 (https://wwwnc.cdc.gov/EID/article/24/1/17-1240-Techapp1.pdf).

the upper respiratory tract of felines may have led to the selection of feline H7N2 virus HA proteins with preferential binding to α2,3-linked sialosides.

Sensitivity to Neuraminidase Inhibitors

To test whether infections with the feline H7N2 viruses could be treated with neuraminidase (NA) inhibitors, we assessed the sensitivity of A/feline/NY/16 and A/chicken/NY/99 to several NA inhibitors (i.e., oseltamivir, zanamivir, and laninamivir) by determining the 50% inhibitory concentration (IC_{50}) of the NA enzymatic activity. We used A/Anhui/1/2013 (H7N9) virus as an NA inhibitor–sensitive control and its NA inhibitor–resistant variant, A/Anhui/1/2013-NA-R294K, as an NA inhibitor–resistant control (online Technical Appendix Table 3). A/feline/NY/16 and A/chicken/NY/99 were sensitive to all of the NA inhibitors tested (Technical Appendix Table 3), consistent with the absence of amino acid residues in the NA protein that are known to confer resistance to NA inhibitors. Hence, NA inhibitors could be used to treat persons infected with feline H7N2 subtype viruses.

Discussion

In our study, we demonstrated that a feline H7N2 subtype virus isolated during an outbreak in an animal shelter in New York in December 2016 replicated well in the respiratory organs of mice and ferrets but did not cause severe symptoms. The efficient replication of the feline H7N2 subtype viruses in the respiratory organs of several mammals, combined with the ability of these viruses to transmit among cats (albeit inefficiently) and to infect 1 person, suggest that these viruses could pose a risk to human health. Close contacts between humans and their pets could lead to the transmission of the feline viruses to humans. To protect public health, shelter animals (where stress and limited space may facilitate virus spread) should be monitored closely for potential outbreaks of influenza viruses.

Our findings of mild disease in mice and ferrets are consistent with the recent report by Belser et al. (*7*) who studied the H7N2 subtype virus isolated from an infected veterinarian. We also assessed feline H7N2 virulence in cats and detected efficient virus replication in both the upper and lower respiratory organs of infected animals, whereas an avian H7N2 subtype virus was detected mainly in the nasal turbinates.

Belser et al. (*7*) reported that intranasal or aerosol infection of ferrets with the H7N2 virus isolated from the infected veterinarian did not result in the seroconversion of co-housed or exposed animals, although nasal wash samples from some of the co-housed ferrets contained low titers of virus; these findings may suggest limited virus transmission that was insufficient to establish a productive infection. In contrast, we detected feline H7N2 virus transmission to co-housed ferrets in 1 of 3 pairs tested; this difference may be explained by the amino acid differences in the PA, HA, and NA proteins of the feline and human H7N2 isolates (online Technical Appendix Table 4) or by the small number of animals used in these studies. We also performed transmission studies in cats and detected feline H7N2 subtype virus transmission via direct contact and respiratory droplets. However, the group size used is a potential limitation of our study.

Cats are not a major reservoir of influenza A viruses, but can be infected naturally or experimentally with influenza viruses of different subtypes (*23*). Serologic surveys suggest high and low rates of seroconversion to seasonal

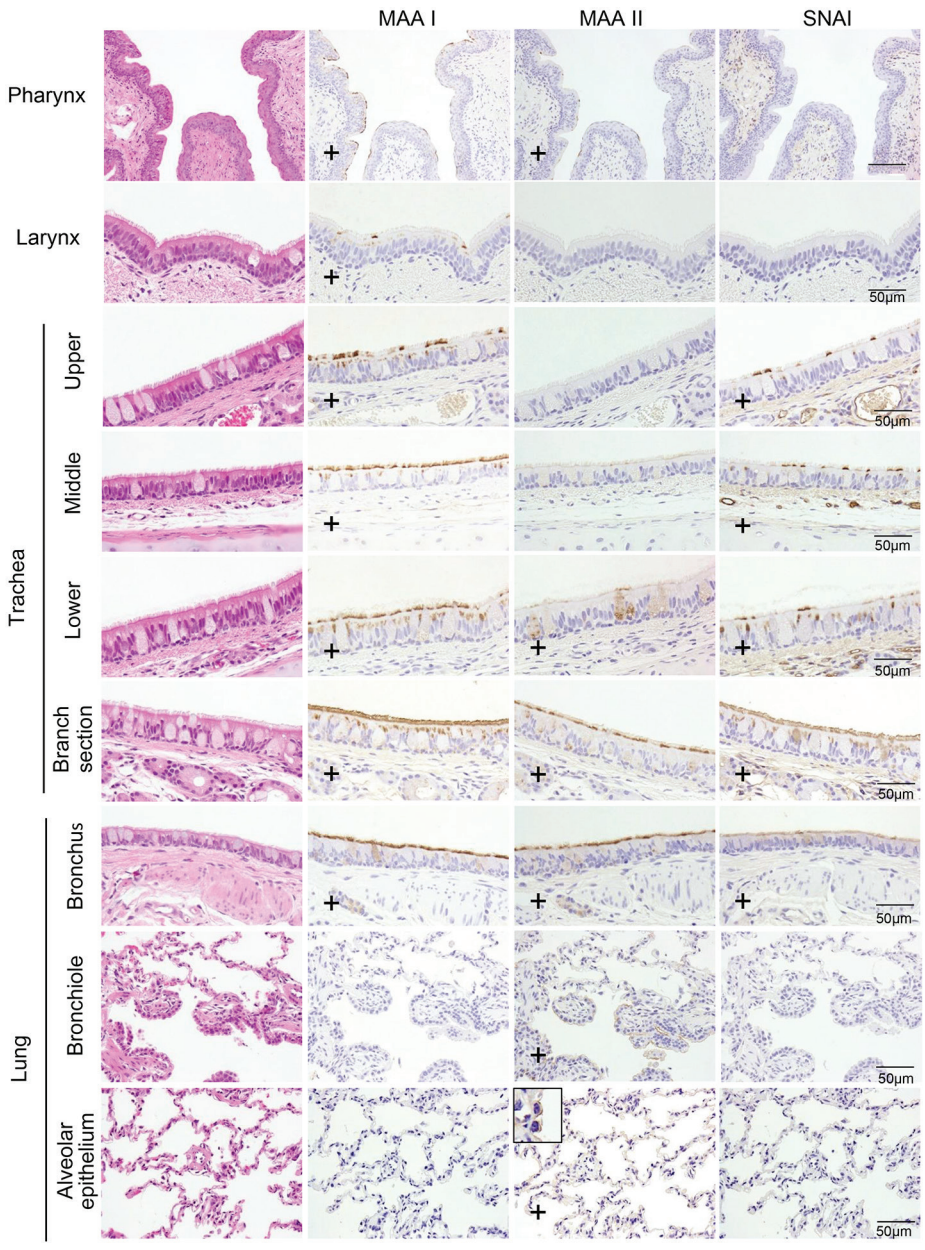

Figure 7. Distribution of α2,3- and α2,6-linked sialosides in the respiratory organs of a cat, New York, NY, USA. The α2,3- and α2,6-linked sialosides in the respiratory organs of a naïve cat were detected with biotinylated Maackia amurensis lectin I or II (MAA I, MAA II) or Sambucus nigra lectin (SNA I), respectively. Inset shows closer view of MAA III binding with alveolar epithelium in the lung. Plus signs (+) indicate that sialosides were detected. Scale bars indicate 50 μm.

human and highly pathogenic avian influenza viruses, respectively. Natural infections most likely result from close contact with infected humans or animals, and most of these infections appear to be self-limiting.

Few cases of human infections with influenza viruses of the H7 subtype were reported until 2013, and they typically caused mild illness; however, infection of a veterinarian with a highly pathogenic avian H7N7 virus had fatal consequences (*24*,*25*). Since 2013, influenza viruses of the H7N9 subtype have caused more than 1,300 laboratory-confirmed infections in humans, with a case-fatality rate of ≈30%. Although the current H7N9 and feline H7N2 subtype viruses do not exclusively bind to human-type receptors and do not transmit efficiently among humans, the spread and biologic properties of these viruses should be monitored carefully.

Acknowledgments

We thank Susan Watson for scientific editing; Peter J. Jester, Alexander Karasin, Kelly E. Moore, Zachary Najacht, Erin M. Plisch, Robert G. Presler, and Backiyalakshmi Ammayappan Venkatachalam for technical assistance; and Philip N. Bochsler for training personnel for animal dissections. We also thank personnel from the Research Animal Resources Center and the Charmany Instructional Facility, University of Wisconsin–Madison, for animal care and technical support.

This work was supported by the NIAID-funded Center for Research on Influenza Pathogenesis (CRIP, HHSN272201400008C) to Y.K.; by NIH grant AI114730 to J.C.P.; by the Japan Initiative for Global Research Network on Infectious Diseases (J-GRID) from the Japan Agency for Medical Research and Development (AMED) to Y.K.; by Leading Advanced Projects for medical innovation (LEAP) from AMED to Y.K.; and by Grants-in-Aid for Scientific Research on Innovative Areas from the Ministry of Education, Culture, Science, Sports, and Technology (MEXT) of Japan (Nos. 16H06429, 16K21723, and 16H06434) to Y.K.

Dr. Hatta is a senior scientist at the Influenza Research Institute at the University of Wisconsin–Madison, Madison, WI. His research focuses on identifying the molecular determinants of influenza virus pathogenicity, with particular emphasis on the pathogenicity of highly pathogenic influenza viruses.

References

1. Wright PF, Neumann G, Kawaoka Y. Orthomyxoviruses. In: Knipe DM, Howley PM, Cohen JI, Griffin DE, Lamb RA, Martin MA, et al., editors. Fields Virology. Sixth ed. Philadelphia, PA, USA: Lippincott Williams & Wilkins; 2013. p. 1186–243.
2. Crawford PC, Dubovi EJ, Castleman WL, Stephenson I, Gibbs EP, Chen L, et al. Transmission of equine influenza virus to dogs. Science. 2005;310:482–5. http://dx.doi.org/10.1126/science.1117950
3. Xie X, Ma K, Liu Y. Influenza A virus infection in dogs: epizootiology, evolution and prevention - A review. Acta Vet Hung. 2016;64:125–39. http://dx.doi.org/10.1556/004.2016.014
4. Song D, Kang B, Lee C, Jung K, Ha G, Kang D, et al. Transmission of avian influenza virus (H3N2) to dogs. Emerg Infect Dis. 2008;14:741–6. http://dx.doi.org/10.3201/eid1405.071471
5. Lee YN, Lee DH, Lee HJ, Park JK, Yuk SS, Sung HJ, et al. Evidence of H3N2 canine influenza virus infection before 2007. Vet Rec. 2012;171:477. http://dx.doi.org/10.1136/vr.100718
6. Fiorentini L, Taddei R, Moreno A, Gelmetti D, Barbieri I, De Marco MA, et al. Influenza A pandemic (H1N1) 2009 virus outbreak in a cat colony in Italy. Zoonoses Public Health. 2011;58:573–81. http://dx.doi.org/10.1111/j.1863-2378.2011.01406.x
7. Belser JA, Pulit-Penaloza JA, Sun X, Brock N, Pappas C, Creager HM, et al. A novel A(H7N2) influenza virus isolated from a veterinarian caring for cats in a New York City animal shelter causes mild disease and transmits poorly in the ferret model. J Virol. 2017;91:e00672-17. http://dx.doi.org/10.1128/JVI.00672-17
8. Spackman E, Senne DA, Davison S, Suarez DL. Sequence analysis of recent H7 avian influenza viruses associated with three different outbreaks in commercial poultry in the United States. J Virol. 2003;77:13399–402.
9. Imai M, Watanabe T, Hatta M, Das SC, Ozawa M, Shinya K, et al. Experimental adaptation of an influenza H5 HA confers respiratory droplet transmission to a reassortant H5 HA/H1N1 virus in ferrets. Nature. 2012;486:420–8.
10. Watanabe T, Kiso M, Fukuyama S, Nakajima N, Imai M, Yamada S, et al. Characterization of H7N9 influenza A viruses isolated from humans. Nature. 2013;501:551–5. http://dx.doi.org/10.1038/nature12392
11. Arafa AS, Yamada S, Imai M, Watanabe T, Yamayoshi S, Iwatsuki-Horimoto K, et al. Risk assessment of recent Egyptian H5N1 influenza viruses. Sci Rep. 2016;6:38388. http://dx.doi.org/10.1038/srep38388
12. Saitou N, Nei M. The neighbor-joining method: a new method for reconstructing phylogenetic trees. Mol Biol Evol. 1987;4:406–25.
13. Felsenstein J. Confidence limits on phylogenies: an approach using the bootstrap. Evolution. 1985;39:783–91. http://dx.doi.org/10.1111/j.1558-5646.1985.tb00420.x
14. Tamura K. Estimation of the number of nucleotide substitutions when there are strong transition-transversion and G+C-content biases. Mol Biol Evol. 1992;9:678–87.
15. Kumar S, Stecher G, Tamura K. MEGA7: Molecular Evolutionary Genetics Analysis version 7.0 for bigger datasets. Mol Biol Evol. 2016;33:1870–4. http://dx.doi.org/10.1093/molbev/msw054
16. Centers for Disease Control and Prevention. H5N1 genetic changes inventory:a tool for influenza surveillance and preparedness. 2012 [cited 2017 Jul 27]. https://www.cdc.gov/flu/pdf/avianflu/h5n1-inventory.pdf
17. Connor RJ, Kawaoka Y, Webster RG, Paulson JC. Receptor specificity in human, avian, and equine H2 and H3 influenza virus isolates. Virology. 1994;205:17–23. http://dx.doi.org/10.1006/viro.1994.1615
18. Gambaryan AS, Tuzikov AB, Piskarev VE, Yamnikova SS, Lvov DK, Robertson JS, et al. Specification of receptor-binding phenotypes of influenza virus isolates from different hosts using synthetic sialylglycopolymers: non-egg-adapted human H1 and H3 influenza A and influenza B viruses share a common high binding affinity for 6′-sialyl(N-acetyllactosamine). Virology. 1997;232:345–50. http://dx.doi.org/10.1006/viro.1997.8572
19. Matrosovich MN, Gambaryan AS, Teneberg S, Piskarev VE, Yamnikova SS, Lvov DK, et al. Avian influenza A viruses differ from human viruses by recognition of sialyloligosaccharides and gangliosides and by a higher conservation of the HA receptor-binding site. Virology. 1997;233:224–34. http://dx.doi.org/10.1006/viro.1997.8580
20. Wang H, Wu X, Cheng Y, An Y, Ning Z. Tissue distribution of human and avian type sialic acid influenza virus receptors in domestic cat. Acta Vet Hung. 2013;61:537–46. http://dx.doi.org/10.1556/AVet.2013.030
21. Said AW, Usui T, Shinya K, Ono E, Ito T, Hikasa Y, et al. A Sero-survey of subtype H3 influenza a virus infection in dogs and cats in Japan. J Vet Med Sci. 2011;73:541–4.
22. Thongratsakul S, Suzuki Y, Hiramatsu H, Sakpuaram T, Sirinarumitr T, Poolkhet C, et al. Avian and human influenza A virus receptors in trachea and lung of animals. Asian Pac J Allergy Immunol. 2010;28:294–301.
23. Harder TC, Vahlenkamp TW. Influenza virus infections in dogs and cats. Vet Immunol Immunopathol. 2010;134:54–60. http://dx.doi.org/10.1016/j.vetimm.2009.10.009
24. Fouchier RA, Schneeberger PM, Rozendaal FW, Broekman JM, Kemink SA, Munster V, et al. Avian influenza A virus (H7N7) associated with human conjunctivitis and a fatal case of acute respiratory distress syndrome. Proc Natl Acad Sci U S A. 2004;101:1356–61. http://dx.doi.org/10.1073/pnas.0308352100
25. Koopmans M, Wilbrink B, Conyn M, Natrop G, van der Nat H, Vennema H, et al. Transmission of H7N7 avian influenza A virus to human beings during a large outbreak in commercial poultry farms in the Netherlands. Lancet. 2004;363:587–93. http://dx.doi.org/10.1016/S0140-6736(04)15589-X

Address for correspondence: Yoshihiro Kawaoka, Influenza Research Institute, Department of Pathobiological Sciences, School of Veterinary Medicine, University of Wisconsin–Madison, 575 Science Dr, Madison, WI 53711, USA; email: yoshihiro.kawaoka@wisc.edu

Article DOI: https://doi.org/10.3201/eid2401.171240

Characterization of a Feline Influenza A(H7N2) Virus

Technical Appendix

Supplementary Methods

Cells and Viruses

Madin-Darby canine kidney (MDCK) cells (obtained from ATCC) were maintained in Eagle's minimal essential medium (MEM) containing 5% newborn calf serum and antimicrobial drugs. Human lung carcinoma epithelial A549 cells were propagated in a 1:1 mixture of Dulbecco's modified Eagle's medium (DMEM) and Ham's F12 medium containing 10% fetal calf serum (FCS) with antimicrobial drugs. Human airway epithelial cells (Calu-3, obtained from Raymond Pickles, University of North Carolina, Chapel Hill, NC, USA) were cultured in DMEM/F12 medium supplemented with 10% FCS and antimicrobial drugs. Chicken embryo fibroblast (CEF) cells were prepared from 10-day-old chicken embryos and cultured in DMEM with 10% FCS and antimicrobial drugs. Cat kidney fibroblast Clone81 (ECACC 90031403) and cat lung Fc2Lu (ECACC 90112712) cells were purchased from the European Collection of Authenticated Cell Cultures (ECACC). Clone81 cells were cultured in DMEM with 10% FCS and antimicrobial drugs. Fc2Lu cells were maintained in MEM with 1% non-essential amino acids (NEAA), 10% FCS, and antimicrobial drugs. All cells were maintained at 37 °C with 5% CO_2 unless otherwise stated.

The viral genomic sequences of the 5 feline H7N2 viruses have been deposited in GenBank under the following accession numbers: A/feline/New York/WVDL-3/2016: MF978390–MF978397; A/feline/New York/WVDL-9/2016: MF978398–MF978405; A/feline/New York/WVDL-14/2016: MF978406–MF978413; A/feline/New York/WVDL-16/2016: MF978414–MF978421; A/feline/New York/WVDL-20/2016: MF978422–MF978429. The sequences of the HA, NA, M, and NS segments of A/chicken/NY/22409–4/1999 virus were available in GenBank (accession nos. AY240896, AY254122, AY241605, and AY241644, respectively) (*1*). We (re)sequenced all 8 viral segments and deposited the sequences of the PB2,

PB1, PA, and NP segments in GenBank under accession nos. MF988320–MF988323. The sequences of the HA and NA segments differed from AY240896 and AY254122 at the nucleotide, but not at the amino acid level, and were deposited in GenBank under accession nos. MF988323 and MF98825, respectively. The sequences of the M and NS segments were identical to AY241605 and AY241644, respectively, and therefore were not submitted to GenBank.

Negative Staining

MDCK cells were infected with A/feline/NY/16 and cultured in 1× MEM containing 0.3% bovine serum albumin and trypsin treated with L-1-tosylamide-2-phenylethyl chloromethyl ketone at 37°C. Forty-eight hours later, the supernatants were harvested and cell debris was removed by centrifugation at 1,750 x *g*. The virion-containing supernatants were adsorbed to Formvar-coated copper mesh grids, negatively stained with 2% phosphotungstic acid solution, and air dried. Digital images of virions were taken with a Tecnai F20 electron microscope (FEI, Tokyo, Japan) at 200 kV.

Animal Experiments

All experiments with mice, ferrets, and cats were performed in accordance with the guidelines set by the Institutional Animal Care and Use Committee at the University of Wisconsin–Madison, which also approved the protocols used (protocol numbers V00806 and V01190). The facilities where this research was conducted are fully accredited by the Association for the Assessment and Accreditation of Laboratory Animal Care International. The animal experiments described in this study were not designed to generate datasets for statistical analysis; hence, the sample size was small and randomization and blinding were not performed.

Immunohistochemistry

Tissues excised from animal organs preserved in 10% phosphate-buffered formalin were processed for paraffin embedding and cut into 5- and 3-μm-thick sections for hematoxylin and eosin staining and immunohistological staining, respectively. One section from each tissue sample was stained using a standard hematoxylin and eosin procedure; another sample was processed for immunohistological staining with a mouse monoclonal or rabbit polyclonal antibody for type A influenza nucleoprotein antigen (prepared in our laboratory) that reacts comparably with all of the viruses used in this study. Specific antigen–antibody reactions were visualized with 3,3′- diaminobenzidine tetrahydrochloride staining by using the DAKO LSAB2

system (Agilent, Santa Clara, CA, USA). Our negative controls (not shown) included sections from mock-infected animals. As a positive control (also not shown), we used formalin-fixed, paraffin-embedded lung sections from humans infected with seasonal influenza viruses.

Detection of α2,3- and α2,6-linked Sialosides in Cat Organs

To detect α2,3- and α2,6-linked sialosides (*2*–*4*), the tissues of a naive cat were fixed in 4% paraformaldehyde–phosphate-buffered saline (PBS) and embedded in paraffin. The paraffin blocks were cut into 3-μm-thick sections and mounted on silane-coated glass slides. The sections were pretreated with 0.05% trypsin (Difco Laboratories, Detroit, MI, USA) at 37°C for 15 min and then with 0.3% hydrogen peroxide at room temperature for 30 min. They were then incubated at 4°C overnight with biotin-conjugated Sambucus nigra lectin I (SNA I; EY Laboratories, San Mateo, CA, USA) to detect α2,6-linked sialosides, or with biotinylated-Maackia amurenis lectin I and II (MAAI and II; Vector Laboratories, Burlingame, CA, USA) to detect α2,3- linked sialosides. After being washed, the sections were incubated with horseradish peroxidase- conjugated streptavidin and visualized by staining with 3,3-diaminobenzidine (DAB).

Neuraminidase Inhibition Assay

Diluted viruses were mixed with different concentrations of oseltamivir carboxylate (the active form of oseltamivir), zanamivir, or laninamivir (all obtained from Daiichi Sankyo Co., Ltd, Tokyo, Japan) (*5*,*6*). Samples were incubated for 30 min at 37°C, followed by the addition of methylumbelliferyl-N-acetylneuraminic acid (Sigma, St Louis, MO) as a fluorescent substrate (*7*,*8*). After incubation for 1 h at 37°C, the reaction was stopped with the addition of sodium hydroxide in 80% ethanol. The fluorescence of the solution was measured at an excitation wavelength of 360 nm and an emission wavelength of 465 nm, and the 50% inhibitory concentration (IC_{50}) was calculated.

Glycan Array Analysis

Glycan array analysis was performed on a glass slide microarray containing 6 replicates of 130 diverse sialic acid-containing glycans, including terminal sequences and intact N-linked and O-linked glycans found on mammalian and avian glycoproteins and glycolipids (*9*). Viruses were amplified in MDCK cells. Supernatants collected from infected cells were centrifuged at 1,462 × *g* for 30 min to remove cell debris. Viruses were inactivated by mixing the supernatants

with 0.1% β-propiolactone (final concentration). Virus supernatant was laid over a cushion of 30% sucrose in PBS, ultracentrifuged at 76,755 × *g* for 2 h at 4°C, and then resuspended in PBS for storage at −80°C. Virus samples (equivalent of 128 hemagglutination units) were incubated on the array surface for 1 h at room temperature, and labeled with mouse monoclonal anti-H7/H1 IgG and goat anti-mouse IgG-Alex Fluor 488 antibodies for sequential 1-hour incubations. Slide scanning to detect virus bound to glycans was conducted using an Innoscan1100AL (Innopsys, Carbonne, France) fluorescent microarray scanner. Fluorescent signal intensity was measured using Mapix (Innopsys, Carbonne, France) and mean intensity minus mean background of 4 replicate spots was calculated. A complete list of the glycans on the array is presented in Technical Appendix, Table 2.

Hemagglutination Inhibition (HI) Assay

To detect hemagglutination inhibition (HI) activity (https://www.cdc.gov/flu/professionals/laboratory/antigenic.htm), serum samples were treated with receptor-destroying enzyme (Denka Seiken Co., Ltd., Tokyo, Japan) at 37°C for 16–20 hours, followed by receptor-destroying enzyme inactivation at 56°C for 30–60 min. The treated sera were serially diluted 2-fold with PBS in 96-well U-bottom microtiter plates (Thermo Scientific, Rochester, NY, USA) and mixed with the amount of virus equivalent to eight hemagglutination units, followed by incubation at room temperature (25°C) for 30 min. After 50 μL of 0.5% turkey erythrocytes was added to the mixtures, they were gently mixed and incubated at room temperature for a further 45 min. HI titers are expressed as the inverse of the highest antibody dilution that inhibited hemagglutination.

Statistical Analyses

We compared the values obtained for each strain, using a 2-way ANOVA, and creating a matrix of contrasts to compare each time-point separately. We then adjusted the p values by using Holm's method to account for family-wise errors; we considered the differences significant if we obtained p values <0.05.

Phylogenetic Analysis

Phylogenetic analyses were carried out for selected avian and human influenza A viruses representing major lineages. The evolutionary history was inferred using the neighbor-joining method (*10*). The optimal trees were selected and the percentages of replicate trees in which the

associated taxa clustered together in the bootstrap test (500 replicates) (*11*) were identified. The trees were drawn to scale, with branch lengths in the same units as those of the evolutionary distances used to infer the phylogenetic tree. The evolutionary distances were computed using the Tamura 3-parameter method (*12*) and are in the units of the number of base substitutions per site. Codon positions included were 1st + 2nd + 3rd + Noncoding. All positions containing gaps and missing data were eliminated. Evolutionary analyses were conducted in MEGA7 (*13*).

Biosafety and Biosecurity

All recombinant DNA protocols were approved by the University of Wisconsin–Madison's Institutional Biosafety Committee after risk assessments were conducted by the Office of Biologic Safety. In addition, the University of Wisconsin–Madison Biosecurity Task Force regularly reviews the research program and ongoing activities of the laboratory. The task force has a diverse skill set and provides support in the areas of biosafety, facilities, compliance, security, and health. Members of the Biosecurity Task Force are in frequent contact with the principal investigator and laboratory personnel to provide oversight and assure biosecurity. The H7N2 viruses used in this study are low pathogenicity avian viruses according to the definition by the US Department of Agriculture and experiments with these viruses can be conducted in Biosafety Level 2+ (BSL2+) containment. For animal experiments with the feline H7N2 viruses, staff wore personal protective equipment including disposable coveralls, double gloves, dedicated shoes with disposable shoe covers, and powered air-purifying respirators that HEPA filter the air for extra protection. Ferret studies were conducted in BSL3 containment. All personnel working in BSL3 containment complete rigorous biosafety, BSL3, and Select Agent (for the US laboratory) training before participating in research studies. The principal investigator participates in training sessions and emphasizes compliance to maintain safe operations and a responsible research environment. The laboratory occupational health plans are in compliance with the policies of the University of Wisconsin–Madison.

References

1. Spackman E, Senne DA, Davison S, Suarez DL. Sequence analysis of recent H7 avian influenza viruses associated with three different outbreaks in commercial poultry in the United States. J Virol. 2003;77:13399–402. PubMed http://dx.doi.org/10.1128/JVI.77.24.13399-13402.2003

2. Shi Y, Wu Y, Zhang W, Qi J, Gao GF. Enabling the 'host jump': structural determinants of receptor-binding specificity in influenza A viruses. Nat Rev Microbiol. 2014;12:822–31. PubMed http://dx.doi.org/10.1038/nrmicro3362

3. Stencel-Baerenwald JE, Reiss K, Reiter DM, Stehle T, Dermody TS. The sweet spot: defining virus-sialic acid interactions. Nat Rev Microbiol. 2014;12:739–49. PubMed http://dx.doi.org/10.1038/nrmicro3346

4. Nicholls JM, Chan RW, Russell RJ, Air GM, Peiris JS. Evolving complexities of influenza virus and its receptors. Trends Microbiol. 2008;16:149–57. PubMed http://dx.doi.org/10.1016/j.tim.2008.01.008

5. Yamashita M. Laninamivir and its prodrug, CS-8958: long-acting neuraminidase inhibitors for the treatment of influenza. Antivir Chem Chemother. 2010;21:71–84. PubMed http://dx.doi.org/10.3851/IMP1688

6. Kamali A, Holodniy M. Influenza treatment and prophylaxis with neuraminidase inhibitors: a review. Infect Drug Resist. 2013;6:187–98. PubMed

7. Gubareva LV, Webster RG, Hayden FG. Comparison of the activities of zanamivir, oseltamivir, and RWJ-270201 against clinical isolates of influenza virus and neuraminidase inhibitor-resistant variants. Antimicrob Agents Chemother. 2001;45:3403–8. PubMed http://dx.doi.org/10.1128/AAC.45.12.3403-3408.2001

8. Kiso M, Kubo S, Ozawa M, Le QM, Nidom CA, Yamashita M, et al. Efficacy of the new neuraminidase inhibitor CS-8958 against H5N1 influenza viruses. PLoS Pathog. 2010;6:e1000786. PubMed http://dx.doi.org/10.1371/journal.ppat.1000786

9. Peng W, de Vries RP, Grant OC, Thompson AJ, McBride R, Tsogtbaatar B, et al. Recent H3N2 viruses have evolved specificity for extended, branched human-type receptors, conferring potential for increased avidity. Cell Host Microbe. 2017;21:23–34. PubMed http://dx.doi.org/10.1016/j.chom.2016.11.004

10. Saitou N, Nei M. The neighbor-joining method: a new method for reconstructing phylogenetic trees. Mol Biol Evol. 1987;4:406–25. PubMed

11. Felsenstein J. Confidence limits on phylogenies: an approach using the bootstrap. Evolution. 1985;39:783–91. PubMed http://dx.doi.org/10.1111/j.1558-5646.1985.tb00420.x

12. Tamura K. Estimation of the number of nucleotide substitutions when there are strong transition-transversion and G+C-content biases. Mol Biol Evol. 1992;9:678–87. PubMed

13. Kumar S, Stecher G, Tamura K. MEGA7: Molecular Evolutionary Genetics Analysis version 7.0 for bigger datasets. Mol Biol Evol. 2016;33:1870–4. PubMed http://dx.doi.org/10.1093/molbev/msw054

14. Kiso M, Iwatsuki-Horimoto K, Yamayoshi S, Uraki R, Ito M, Nakajima N, et al. Emergence of oseltamivir-resistant h7n9 influenza viruses in immunosuppressed cynomolgus macaques. J Infect Dis. 2017;216:582–93. PubMed http://dx.doi.org/10.1093/infdis/jix296

Technical Appendix Table 1. Antigenic characterization of H7 viruses by use of monoclonal antibodies

		Hemagglutination inhibition (HI) titers*							
		Mouse monoclonal antibody against							
		HA from A/Seal/Mass/1/80 (H7N7)				HA from A/Netherlands/ 219/03 (H7N7)	HA from A/Anhui/1/2013 (H7N9)		
Virus	Subtype	46/6	55/3	58/2	8/4	10C6	2–20–20	3–7-19	19–17–20
A/feline/New York/WVDL-14/2016 (Feline/NY/16)	H7N2	<50	<50	<50	100	400	200	100	400
A/chicken/NY/22409–4/1999 (Chicken/NY/99)		<50	800	<50	<50	400	200	100	200
A/duck/Hong Kong/301/1978		<50	50	1600	<50	<50	<50	<50	<50
A/turkey/England/1963	H7N3	<50	3200	800	<50	<50	<50	<50	<50
A/turkey/Oregon/1971		<50	50	200	<50	<50	200	<50	400
A/turkey/Tennessee/1/1976		<50	<50	100	<50	<50	<50	<50	<50
A/chicken/Japan/1925	H7N7	<50	<50	400	<50	<50	<50	<50	<50
A/equine/Prague/1/1956		<50	<50	<50	<50	200	<50	<50	<50
A/equine/New Market/1/1977		<50	<50	<50	<50	1600	<50	<50	<50
A/seal/Massachusetts/1/1980		3200	6400	3200	800	800	800	200	800
A/duck/Taiwan/103/1993		<50	<50	400	<50	<50	<50	<50	<50
A/duck/Gunma/466/2011	H7N9	<50	100	1600	<50	<50	100	<50	200
A/Anhui/1/2013		1600	3200	800	<50	800	200	50	400

*Hemagglutination inhibition (HI) assays were carried out as follows: 2-fold serial dilutions of antibodies were mixed with the amount of virus equivalent to 8 hemagglutination units of virus in 96-well U-bottom microtiter plates, followed by incubation at room temperature for 60 min. After an equal volume of 0.5% chicken red blood cells was added, the mixtures were gently mixed and then incubated for a further 60 min at 4°C. HI titers were determined as the inverse of the highest antibody dilution that inhibited the hemagglutination.

Technical Appendix Table 2. List of glycans used for arrays

No	M#	S#	Common Name	Linkage	NeuAC/NeuGc(A/B), both -C	Structure
1	**M040**	**M040**	Galβ(1–4)-GlcNAcβ-ethyl-NH2	–	–	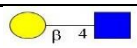
2	M221	WJ-5–149–1	Galβ(1-4)GlcNAcβ(1-3)Galβ(1-3)GalNAca-Thr-NH2	–	–	
3	M222	152Sp14	Galβ(1-4)GlcNAcβ(1-6)[Galβ(1-3)]-GalNAca-Thr-NH2	–	–	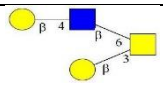
4	M223	144Sp14	Galβ(1-4)GlcNAcβ(1-3)GalNAca-Thr-NH2	–	–	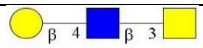
5	M224	21Sp14	Galβ(1-4)GlcNAcβ(1-3)[Galβ(1-4)GlcNAcβ(1-6)]-GalNAcα-Thr-NH2	–	–	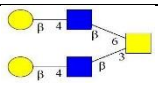
6	M225	119Sp14	Galβ(1-4)GlcNAcβ(1-6)GalNAcα-Thr-NH2	–	–	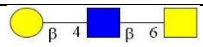
7	**M009**	**M009**	Galβ(1–4)-GlcNAcβ(1–2)-Manα(1-3)-[Galβ(1–4)-GlcNAcβ(1–2)-Manα(1–6)]-Manβ(1–4)-GlcNAcβ(1-4)-GlcNAcβ-Asn-NH2	–	–	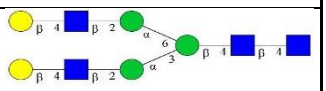
8	M226	375Sp22	Galβ(1-4)GlcNAcβ(1-2)Manα(1-3)[Galβ(1-4)GlcNAcβ(1-2)Manα(1-6)]-Manβ(1-4)GlcNAcβ(1-4)[Fucα(1-6)]-GlcNAcβ-Asn-Ser-Thr-NH2	–	–	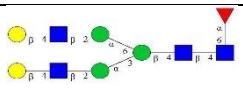

No	M#	S#	Common Name	Linkage	NeuAC/NeuGc(A/B), both -C	Structure
9	M227	487Sp19	Galβ(1-4)GlcNAcβ(1-2)Manα(1-3){Galβ(1-4)GlcNAcβ(1-2)[Galβ(1-4)GlcNAcβ(1-2)]-Manα(1-6)}-Manβ(1-4)GlcNAcβ(1-4)GlcNAcβ-Asn-Lys-NH2	–	–	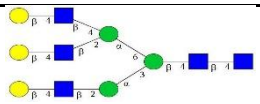
10	M228	517Sp	Galβ(1-4)GlcNAcβ(1-2)Manα(1-3){Galβ(1-4)GlcNAcβ(1-2)[Galβ(1-4)GlcNAcβ(1-2)]-Manα(1-6)}-Manβ(1-4)GlcNAcβ(1-4)[Fucα(1-6)]-GlcNAcβ-(Lys-Val-Ala)Asn-Lys-ThrNH2	–	–	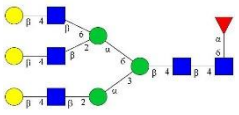
11	**M001**	**M001**	NeuAcα(2-3)Galβ(1-4)6-O-sulfoGlcNAcβ-propyl-NH2	3	A	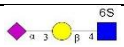
12	**M037**	**M037**	NeuAcα(2–3)-Galβ(1–4)-[Fucα(1–3)]-6-O-sulfo-GlcNAcβ-propyl-NH2	3	A	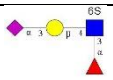
13	**M039**	**M039**	NeuAcα(2–3)-6-O-sulfo-Galβ(1–4)- GlcNAcβ-ethyl-NH2	3	A	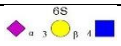
14	**M036**	**M036**	NeuAcα(2–3)-6-O-sulfo-Galβ(1–4)-[Fucα(1–3)]-GlcNAcβ-propyl-NH2	3	A	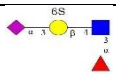
15	**M038**	**M038**	NeuAcα(2–3)-Galβ(1–3)-6-O-sulfo-GlcNAcβ-propyl-NH2	3	A	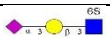

No	M#	S#	Common Name	Linkage	NeuAC/NeuGc(A/B), both -C	Structure
16	**M011**	**M011**	NeuAcα(2–3)-Galβ(1–4)-Glcβ-ethyl-NH_2	3	A	
17	**M012**	**M012**	NeuAcα(2–3)-Galβ(1–4)-GlcNAcβ-ethyl-NH_2	3	A	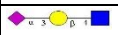
18	**M014**	**M014**	NeuAcα(2–3)-Galβ(1–4)-GlcNAcβ(1-3)-Galβ(1–4)-GlcNAcβ-ethyl-NH_2	3	A	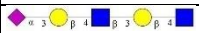
19	**M035**	**M035**	NeuAcα(2–3)-Galβ(1–4)-GlcNAcβ(1-3)-Galβ(1–4)-GlcNAcβ(1–3)-Galβ(1-4)-	3	A	
20	**M013**	**M013**	NeuAcα(2–3)-GalNAcβ(1–4)-GlcNAcβ-ethyl-NH_2	3	A	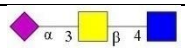
21	**M010**	**M010**	NeuAcα(2–3)-Galβ(1–3)-GlcNAcβ-ethyl-NH_2	3	A	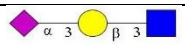
22	**M032**	**M032**	NeuAcα(2–3)-Galβ(1–3)-GlcNAcβ(1-3)-Galβ(1–4)-GlcNAcβ-ethyl-NH_2	3	A	
23	**M033**	**M033**	NeuAcα(2–3)-Galβ(1–3)-GlcNAcβ(1-3)-Galβ(1–3)-GlcNAcβ-ethyl-NH_2	3	A	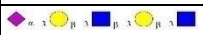
24	**M028**	**M028**	NeuAcα(2–3)-Galβ(1–3)-GalNAcβ(1-3)-Galα(1–4)-Galβ(1–4)-Glcβ-ethyl-	3	A	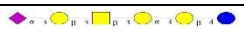
25	**M045**	**M045**	NeuAcα(2–3)-Galβ(1–3)-GalNAcα-Thr-NH_2	3	A	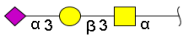

26	M120	WJ-6–121–1	3′ NeuAc LN Core 1 (1163)	3	A	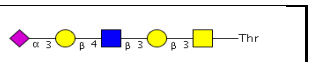
27	M128	WJ-6–153–1	3′ NeuAc DiLN Core 1 (1528)	3	A	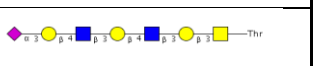
28	M153	WJ-8–145–1	3′ NeuAc TriLN Core 1 (1894)	3	A	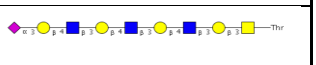
29	M142	WJ-8–101–1	3′ NeuAc TetraLN Core 1 (2259)	3	A	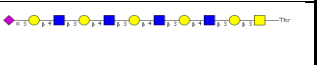
30	M143	WJ-8–103–1	3′ NeuAc PentaLN Core 1 (2624)	3	A	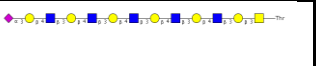
31	**M050**	**M050**	NeuAcα(2–3)-Galβ(1–4)-GlcNAcβ(1-6)-[Galβ(1–3)]-GalNAcα-Thr-NH_2	3	A	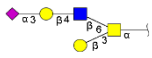
32	**M053**	**M053**	NeuAcα(2–3)-Galβ(1–4)-GlcNAcβ(1-3)-Galβ(1–4)-GlcNAcβ(1–6)-[Galβ(1-	3	A	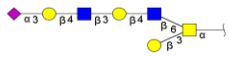
33	**M202**	WJ-9–41–1	3′ NeuAc TriLN Core 2 (1894)	3	A	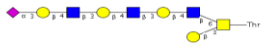
34	M152	WJ-8–141–1	3′ NeuAc TetraLN Core 2 (2259)	3	A	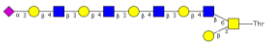
35	M149	WJ-8–131–1	3′ NeuAc PentaLN Core 2 (2624)	3	A	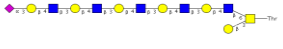
36	**M195**	WJ-9–13–1	3′ NeuAc TetraLN TriLN Core 2 (3645)	3	A	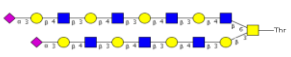

37	M156	WJ-8–155–1	3′ NeuAc PentaLN TetraLN Core 2 (4376)	3	A	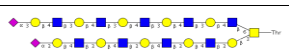
38	**M055**	**M055**	NeuAcα(2–3)-Galβ(1–4)-GlcNAcβ(1-3)-GalNAcα-Thr-NH_2	3	A	
39	**M057**	**M057**	NeuAcα(2–3)-Galβ(1–4)-GlcNAcβ(1-3)-Galβ(1–4)-GlcNAcβ(1–3)-GalNAcα-Thr-NH_2	3	A	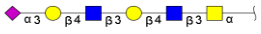
40	**M186**	WJ-8–99–1	3′ NeuAc TriLN Core 3 (1732)	3	A	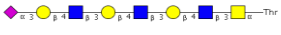
41	**M178**	WJ-8–83–1	3′ NeuAc TetraLN Core 3 (2097)	3	A	
42	**M177**	WJ-8–77–1	3′ NeuAc PentaLN Core 3 (2462)	3	A	
43	**M059**	**M059**	NeuAcα(2–3)-Galβ(1–4)-GlcNAcβ(1-3)-[NeuAcα(2–3)-Galβ(1–4)-GlcNAcβ(1–6)]-	3	A	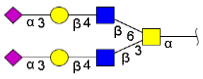
44	**M061**	**M061**	NeuAcα(2–3)-Galβ(1–4)-GlcNAcβ(1-3)-Galβ(1–4)-GlcNAcβ(1–3)-[NeuAcα(2–3)-	3	A	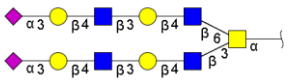
45	**M185**	WJ-8–97–1	3′ NeuAc TriLN Core4 (3118)	3	A	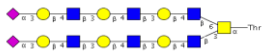
46	**M180**	WJ-8–87–1	3′ NeuAc TetraLN Core4 (3848)	3	A	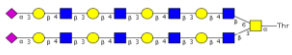
47	**M179**	WJ-8–85–1	3′ NeuAc PentaLN Core4 (4579)	3	A	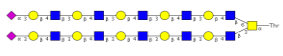

48	**M182**	WJ-8–91–1	3′ NeuAc TetraLN Core6 (2097)	3	A	
49	**M184**	WJ-8–95–1	3′ NeuAc PentaLN Core6 (2462)	3	A	
50	**M102**	WJ-10–71–1	3′ NeuAc LecLN I-Antigen(2104)	3	A	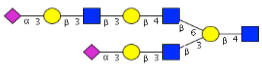
51	**M098**	WJ-10–61–1	3′ NeuAc TriLN I-Antigen (2856)	3	A	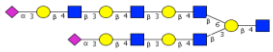
52	**M026**	**M026**	NeuAcα(2–3)-Galβ(1–4)-GlcNAcβ(1-2)-Manα(1–3)-[NeuAcα(2–3)-Galβ(1-	3	A	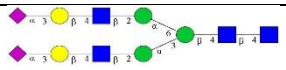
53	**M041**	**M041**	NeuAcα(2–3)-Galβ(1–4)-GlcNAcβ(1-3)-Galβ(1–4)-GlcNAcβ(1–2)-Manα(1–3)-	3	A	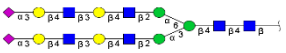
54	**M043**	**M043**	NeuAcα(2–3)-Galβ(1–4)-GlcNAcβ(1-3)-Galβ(1–4)-GlcNAcβ(1–3)-Galβ(1-	3	A	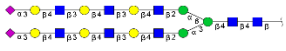
55	**M107**	WJ-5–21–1	3′ NeuAc DiLN Bi-(3594)	3	A	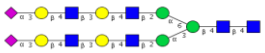
56	**M110**	WJ-5–35–1	3′ NeuAc TriLN Bi-(4324)	3	A	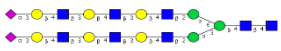
57	**M112**	WJ-5–39–1	3′ NeuAc TetraLN Bi-(4828)	3	A	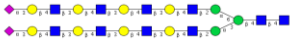
58	**M114**	WJ-5–45–1	3′ NeuAc PentaLN Bi-(5556)	3	A	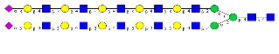

59	M132	WJ-6–41–1	3′ NeuAc TriLN Bi-CF(4470)	3	A	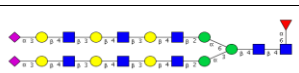
60	M122	WJ-6–13–1	3′ NeuAc TetraLN Bi-CF(5200)	3	A	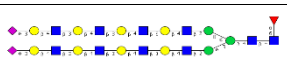
61	M118	WJ-6–117–1	3′ NeuAc DiLN Tri-(4615)	3	A	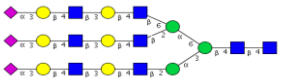
62	M119	WJ-6–119–1	3′ NeuAc TriLN Tri-(5716)	3	A	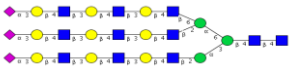
63	M141	WJ-7–47–1	3′ NeuAc TetraLN Tri-(6808)	3	A	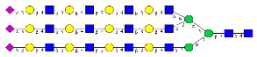
64	M125	WJ-6–149–1	3′ NeuAc DiLN Tri-CF(4761)	3	A	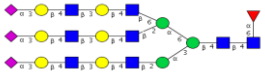
65	M127	WJ-6–151–1	3′ NeuAc TriLN Tri-CF(5858)	3	A	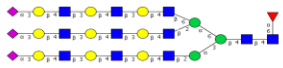
66	**M068**	701_WJ-10–91–1	Gn/3′SLN/3′SLN-TriN	3	A	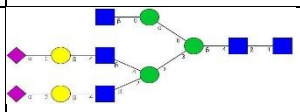
67	**M031**	**M031**	NeuAcα(2–3)-[GalNAcβ(1–4)]-Galβ(1–4)-GlcNAcβ-ethyl-NH_2	3	A	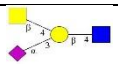
68	**M016**	**M016**	NeuAcα(2–3)-[GalNAcβ(1–4)]-Galβ(1–4)-Glcβ-ethyl-NH_2	3	A	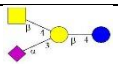
69	**M017**	**M017**	Galβ(1–3)-GalNAcβ(1–4)-[NeuAcα(2–3)]-Galβ(1–4)-Glcβ-ethyl-NH_2	3	A	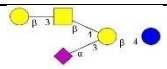

70	**M002**	**M002**	NeuAcα(2–3)-Galβ(1–4)-[Fucα(1–3)]-GlcNAcβ-propyl-NH_2	3	A	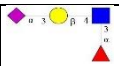
71	**M029**	**M029**	NeuAcα(2–3)-Galβ(1–3)-[Fucα(1–4)]-GlcNAcβ(1–3)-Galβ(1–4)-[Fucα(1- 3)]-	3	A	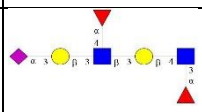
72	**M022**	**M022**	NeuAcα(2–3)-Galβ(1–4)-[Fucα(1–3)]-GlcNAcβ(1–3)-Galβ(1–4)-[Fucα(1- 3)]-	3	A	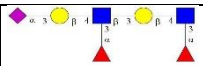
73	**M015**	**M015**	NeuAcα(2–3)-Galβ(1–4)-[Fucα(1–3)]-GlcNAcβ(1–3)-Galβ(1–4)-[Fucα(1-3)]-GlcNAcβ(1–3)-	3	A	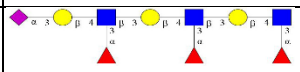
74	**M206**	WJ-9–7-1	3′ SLeX TriLN Core 1(2332)	3	A	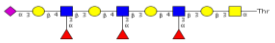
75	M147	WJ-8–127–1	3′ SLeX TriLN Core 3(2170)	3	A	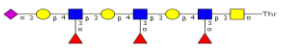
76	M146	WJ-8–125–1	3′ SLeX TriLN Core 4(3994)	3	A	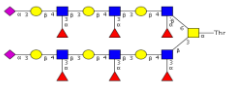
77	M219	WJ-119–1	NeuAcα(2-3)Galβ(1-4)[Fucα(1-3)]-GlcNAcβ(1-2)Mana(1-3)[NeuAcα(2-3)Galβ(1-4)[Fucα(1-3)]-GlcNAcβ(1-2)Mana(1-6)]-Manβ(1-4)GlcNAcβ(1-4)GlcNAcβ-(Lys-Val-Ala)Asn-(Lys-Thr)NH2	3	A	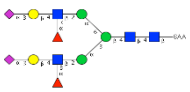
78	M215	WJ-12–79–1	NeuAc(2–6)-Galb(1–4)-(6S)GlcNacb-ethyl-NH2	6	A	
	M003	**M003**	NeuAcα(2–6)-Galβ(1–4)-6-O-sulfo-GlcNAcβ-propyl-NH_2	6	A	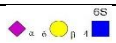

80	**M018**	**M018**	NeuAcα(2–6)-Galβ(1–4)-Glcβ-ethyl-NH_2	6	A	
81	**M019**	**M019**	NeuAcα(2–6)-Galβ(1–4)-GlcNAcβ-ethyl-NH_2	6	A	
82	**M021**	**M021**	NeuAcα(2–6)-Galβ(1–4)-GlcNAcβ(1-3)-Galβ(1–4)-GlcNAcβ-ethyl-NH_2	6	A	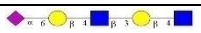
83	**M025**	**M025**	NeuAcα(2–6)-Galβ(1–4)-GlcNAcβ(1-3)-Galβ(1–4)-GlcNAcβ(1–3)-Galβ(1-4)-GlcNAcβ-	6	A	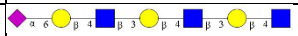
84	**M020**	**M020**	NeuAcα(2–6)-GalNAcβ(1–4)-GlcNAcβ-ethyl-NH_2	6	A	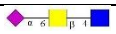
85	M121	WJ-6–123–1	6’ NeuAc LN Core 1 (1163)	6	A	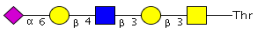
86	M129	WJ-6–155–1	6’ NeuAc DiLN Core 1 (1528)	6	A	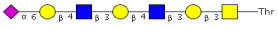
87	M154	WJ-8–147–1	6’ NeuAc TriLN Core 1 (1894)	6	A	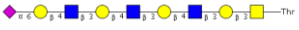
88	M135	WJ-7–149–1	6’ NeuAc TetraLN Core 1 (2259)	6	A	
89	M148	WJ-8–13–1/WJ-7–107-1	6’ NeuAc PentaLN Core 1 (2624)	6	A	
90	**M051**	**M051**	NeuAcα(2–6)-Galβ(1–4)-GlcNAcβ(1-6)-[Galβ(1–3)]-GalNAcα-Thr-NH_2	6	A	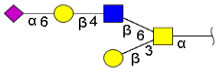

91	**M054**	**M054**	NeuAcα(2–6)-Galβ(1–4)-GlcNAcβ(1-3)-Galβ(1–4)-GlcNAcβ(1–6)-[Galβ(1-	6	A	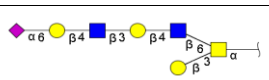
92	**M201**	WJ-9–39–1	6’ NeuAc TriLN Core 2 (1894)	6	A	
93	M159	WJ-8–23–1	6’ NeuAc TetraLN Core 2 (2259)	6	A	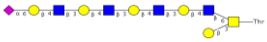
94	M157	WJ-8–17–1	6’ NeuAc PentaLN Core 2 (2624)	6	A	
95	M163	WJ-8–33–1	6’ NeuAc TetraLN TriLN Core 2 (3645)	6	A	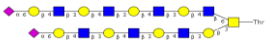

96	M161	WJ-8–29–1	6’ NeuAc PentaLN TetraLN Core 2 (4376)	6	A	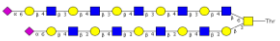
97	**M056**	**M056**	NeuAcα(2–6)-Galβ(1–4)-GlcNAcβ(1-3)-GalNAcα-Thr-NH_2	6	A	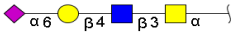
98	**M058**	**M058**	NeuAcα(2–6)-Galβ(1–4)-GlcNAcβ(1-3)-Galβ(1–4)-GlcNAcβ(1–3)-GalNAcα-Thr-NH_2	6	A	
99	M172	WJ-8–65–1	6’ NeuAc TriLN Core 3 (1732)	6	A	
100	M166	WJ-8–49–1	6’ NeuAc TetraLN Core 3 (2097)	6	A	
101	M164	WJ-8–35–1	6’ NeuAc PentaLN Core 3 (2462)	6	A	

102	**M060**	**M060**	NeuAcα(2–6)-Galβ(1–4)-GlcNAcβ(1-3)-[NeuAcα(2–6)-Galβ(1–4)-GlcNAcβ(1–6)]-	6	A	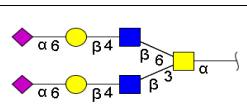
103	**M062**	**M062**	NeuAcα(2–6)-Galβ(1–4)-GlcNAcβ(1-3)-Galβ(1–4)-GlcNAcβ(1–3)-[NeuAcα(2–6)-	6	A	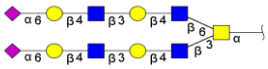
104	M174	WJ-8–73–1	6’ NeuAc TriLN Core4 (3118)	6	A	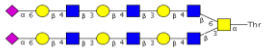
105	M170	WJ-8–61–1	6’ NeuAc TetraLN Core4 (3848)	6	A	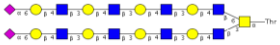
106	M168	WJ-8–57–1	6’ NeuAc PentaLN Core4 (4579)	6	A	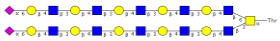
107	**M181**	WJ-8–89–1	6’ NeuAc TetraLN Core6 (2097)	6	A	
108	**M183**	WJ-8–93–1	6’ NeuAc PentaLN Core6 (2462)	6	A	
109	**M097**	WJ-10–59–1	6’ NeuAc TriLN I-Antigen (2856)	6	A	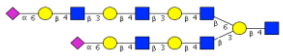
110	**M104**	WJ-10–77–1	6’ NeuAc DiLN I-Antigen (2104)	6	A	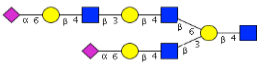
111	**M006**	**M006**	Galβ(1–4)-GlcNAcβ(1–2)-Manα(1-3)-[NeuAcα(2–6)-Galβ(1–4)-GlcNAcβ(1–2)-	6	A	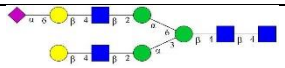
112	**M007**	**M007**	NeuAcα(2–6)-Galβ(1–4)-GlcNAcβ(1-2)-Manα(1–3)-[Galβ(1–4)-GlcNAcβ(1–2)-	6	A	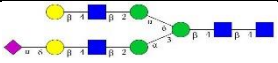

113	**M008**	**M008**	GlcNAcβ(1–2)-Manα(1–3)-[NeuAcα(2–6)-Galβ(1–4)-GlcNAcβ(1–2)-Manα(1–6)]-	6	A	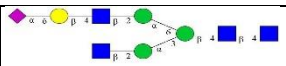
114	**M004**	**M004**	NeuAcα(2–6)-Galβ(1–4)-GlcNAcβ(1-2)-Manα(1–3)-[NeuAcα(2–6)-Galβ(1-	6	A	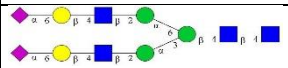
115	**M042**	**M042**	NeuAcα(2–6)-Galβ(1–4)-GlcNAcβ(1-3)-Galβ(1–4)-GlcNAcβ(1–2)-Manα(1–3)-[NeuAcα(2–6)-Galβ(1–4)-GlcNAcβ(1–3)-Galβ(1–4)-GlcNAcβ(1–2)-Manα(1–6)]-Manβ(1- 4)-GlcNAcβ(1–4)-GlcNAcβ-Asn- ^{NH}2	6	A	
116	**M109**	WJ-5–33–1	6’ NeuAc DiLN Bi-(3594)	6	A	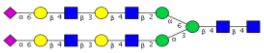
117	**M044**	**M044**	NeuAcα(2–6)-Galβ(1–4)-GlcNAcβ(1-3)-Galβ(1–4)-GlcNAcβ(1–3)-Galβ(1-	6	A	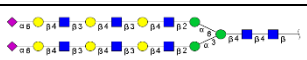
118	**M089**	JP-3–8-1	6’ NeuAc TriLN Bi-(4324)	6	A	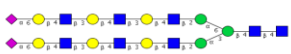
119	**M081**	JP-3–12–1	6’ NeuAc TetraLN Bi-(4828)	6	A	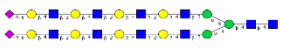
120	**M083**	JP-3–16–1	6’ NeuAc PentaLN Bi-(5556)	6	A	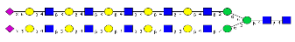
121	**M085**	JP-3–20–2	6’ NeuAc DiLN Bi-CF(3740)	6	A	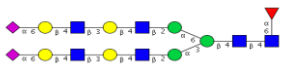
122	**M087**	JP-3–24–1	6’ NeuAc TriLN Bi-CF(4470)	6	A	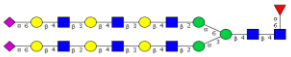

123	M131	WJ-6–25–1	6' NeuAc TetraLN Bi-CF(5200)	6	A	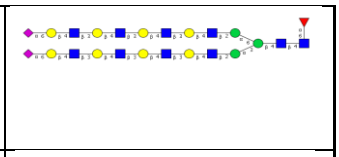
124	M123	WJ-6–133–1	6' NeuAc DiLN Tri-(4615)	6	A	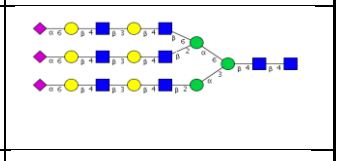
125	M134	WJ-7–13–1	6' NeuAc DiLN Tri-CF(4761)	6	A	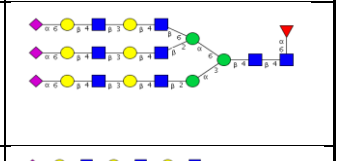
126	M136	WJ-7–15–1	6' NeuAc TriLN Tri-CF(5858)	6	A	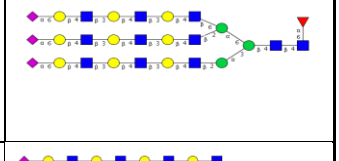
127	M138	WJ-7–35–1	6' NeuAc TetraLN Tri-CF(6952)	6	A	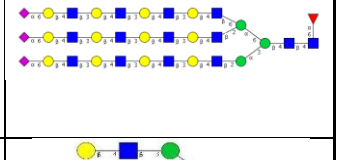
128	**M065**	112_WJ-10–147–1	LN/6'SLN/6'SLN-TriN	6	A	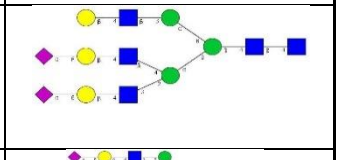
129	**M067**	128_WJ-10–149–1	6'SLN/LeX/LeX-TriN	6	A	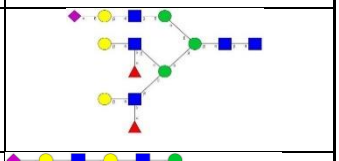
30	**M063**	047_WJ-10–145–1	6'SLNLN/LeX/LeX-TriN	6	A	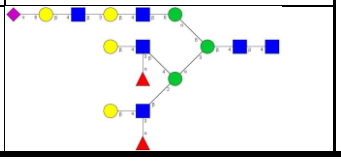

Technical Appendix Table 3. Virus sensitivity to NA inhibitors

	IC_{50} value*			
NA inhibitors	Chicken/NY/99	Feline/NY/16	A/Anhui/1/2013[§] (H7N9)	A/Anhui/1/2013 -NA-R294K[¶] (H7N9)
Oseltamivir carboxylate[†]	1.6	1.0	3.6	64,000
Zanamivir	5.6	8.2	8.1	340
Laninamivir[‡]	15	17.5	3.4	210

*IC_{50} value: mean nmol/L of duplicate reactions.
[†]Oseltamivir carboxylate is the active form of oseltamivir.
[‡]Laninamivir is the active form of laninamivir octanoate.
[§]A/Anhui/1/2013 (H7N9): NA inhibitor-sensitive virus.
[¶]A/Anhui/1/2013-NA-R294K (H7N9): NA inhibitor-resistant virus (14).

Technical Appendix Table 4. Amino acid differences among A/feline/NY/16 virus and human H7N2 isolate (A/New York/108/2016)

Virus	Amino acid positions in the viral proteins					
	PA	HA			NA	
	57	9	127	156	40	362
A/feline/NY/16	Q	T	S	T	Y	R
A/New York/108/2016*	R	I	N	A	H	K

*The sequences were obtained from GISAID (accession nos. EPI944622–EPI944629). PA, polymerase; HA, hemagglutinin; NA, neuraminidase.

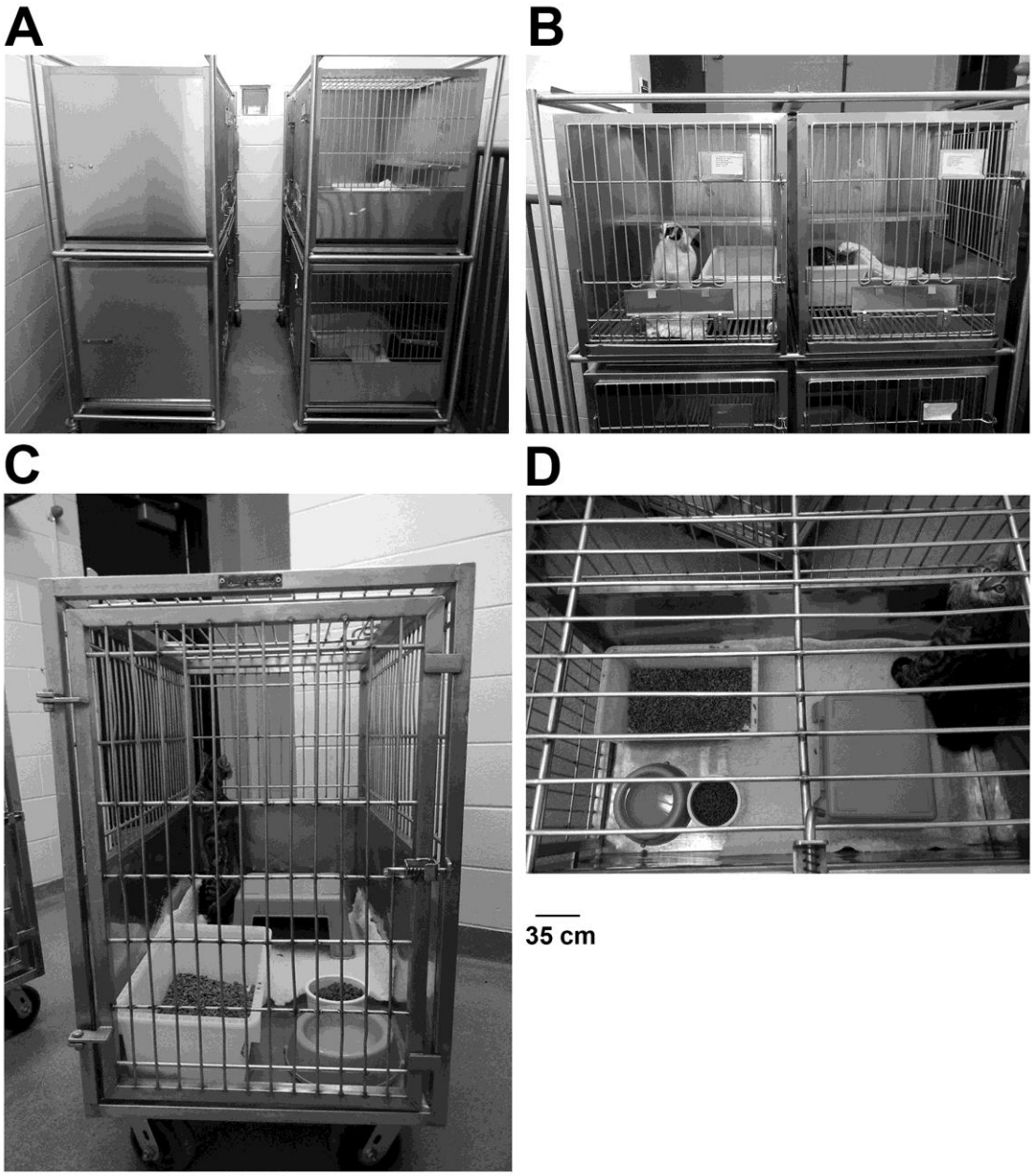

Technical Appendix Figure 1. Cage settings for virus transmission studies in cats. All cat transmission experiments were conducted at the Charmany Instructional Facility, School of Veterinary Medicine, University of Wisconsin–Madison, under controlled conditions of temperature and humidity. (A and B) Cages and racks used for respiratory droplet transmission studies. Cats were housed individually in regular cat cages. The two racks holding infected and naïve cats were spaced 35 cm apart to prevent direct and indirect contact between animals while allowing respiratory droplet transmission of influenza viruses. (C and D) Cages used for direct contact transmission studies. Large dog transporter cages with a perch/resting platform were used. One infected and one naïve cat were housed together in one cage.

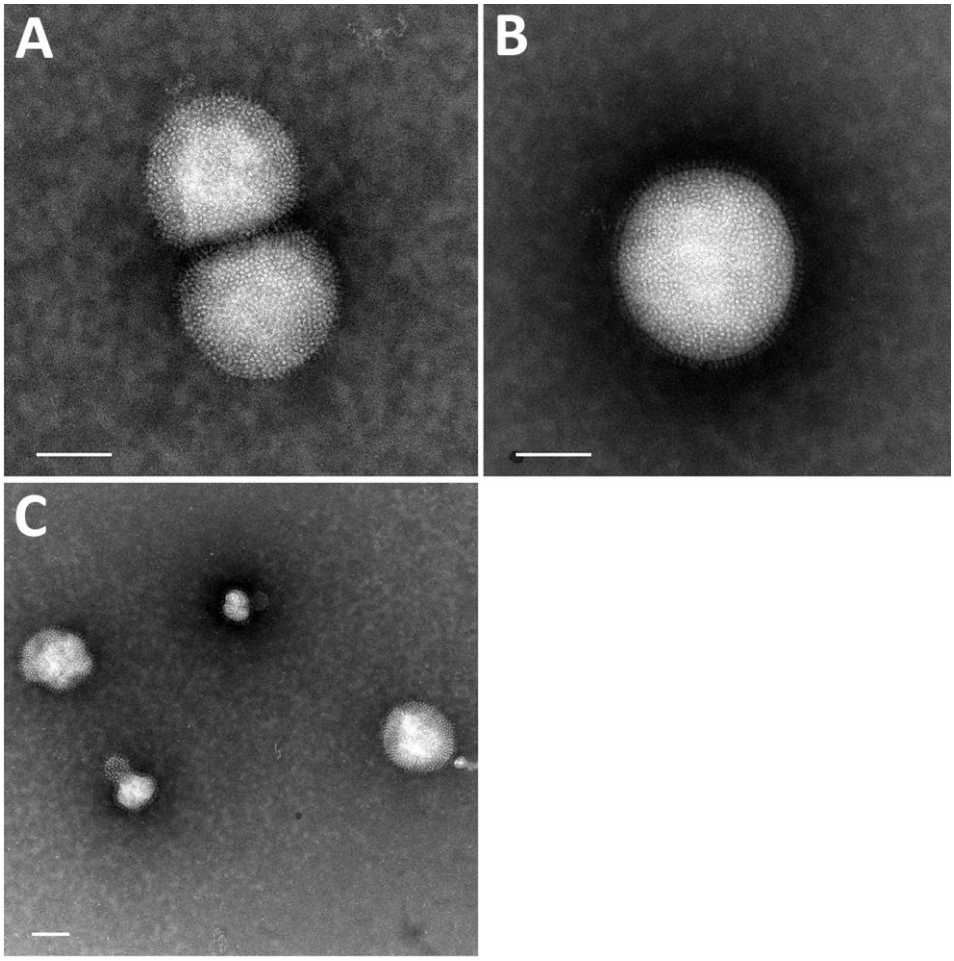

Technical Appendix Figure 2. Images of feline H7N2 virions observed by negative-staining electron microscopy. Virions negatively stained with 2% phosphotungstic acid solution were observed under an electron microscope. (A and B) Higher magnification of virus particles. (C) Lower magnification of virus particles. Scale bar = 100 nm.

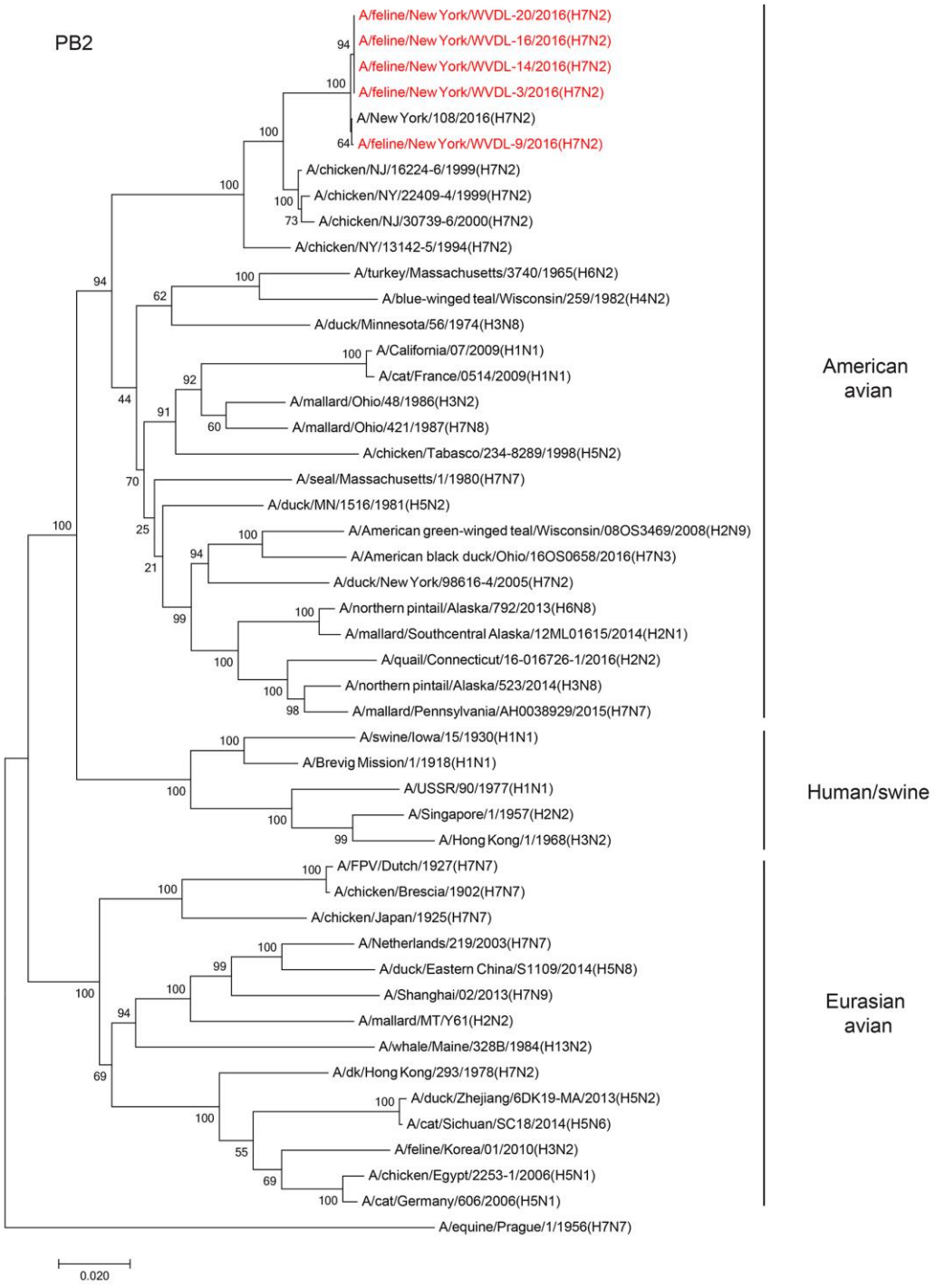

Technical Appendix Figure 3. Phylogenetic tree of influenza A viral PB2 segments. The optimal tree with the sum of branch length = 1.59092622 is shown. The analysis involved 48 nt sequences. The final dataset contained a total of 2,260 positions.

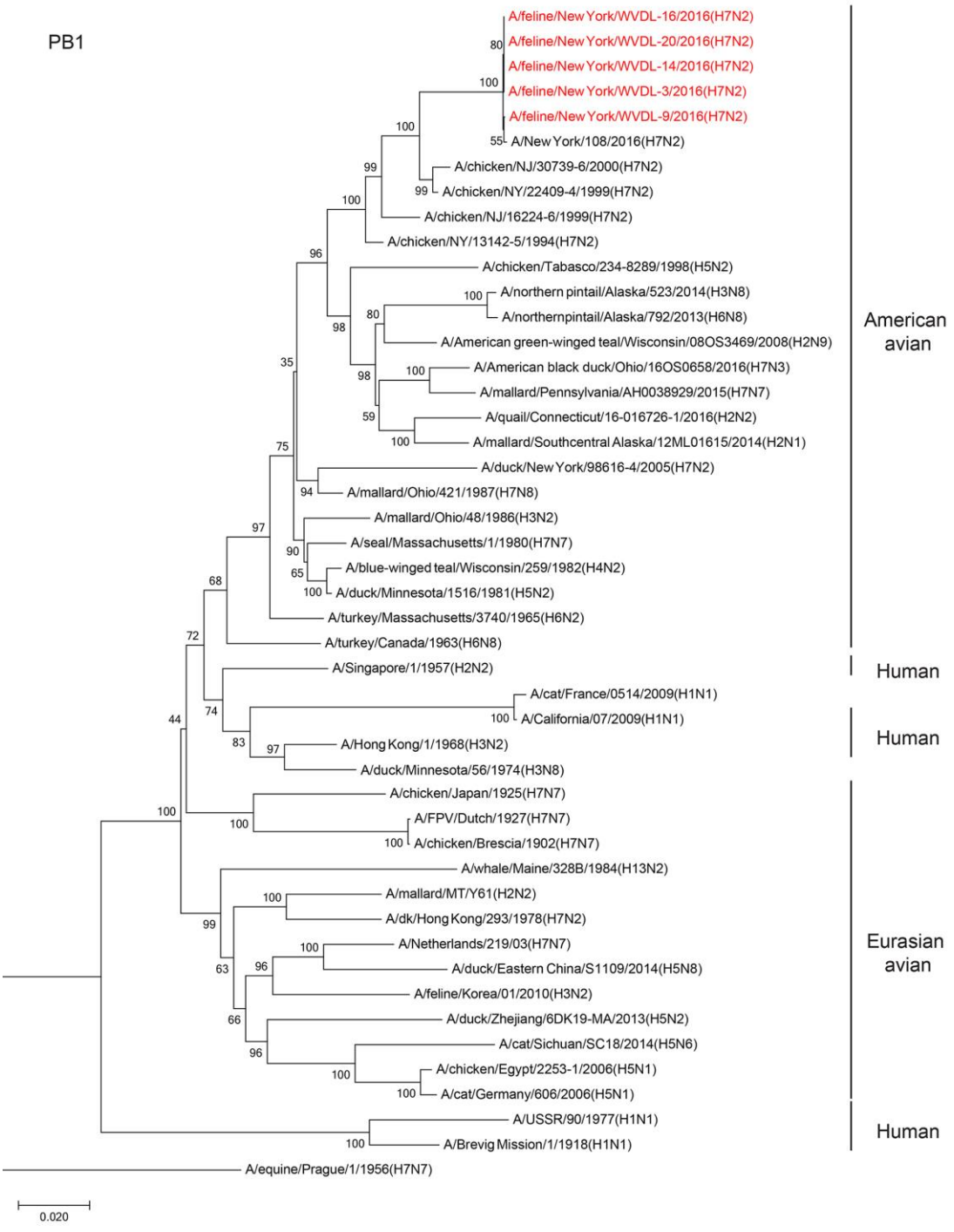

Technical Appendix Figure 4. Phylogenetic tree of influenza A viral PB1 segments. The optimal tree with the sum of branch length = 1.3928728 is shown. The analysis involved 47 nt sequences. The final dataset contained a total of 2,263 positions.

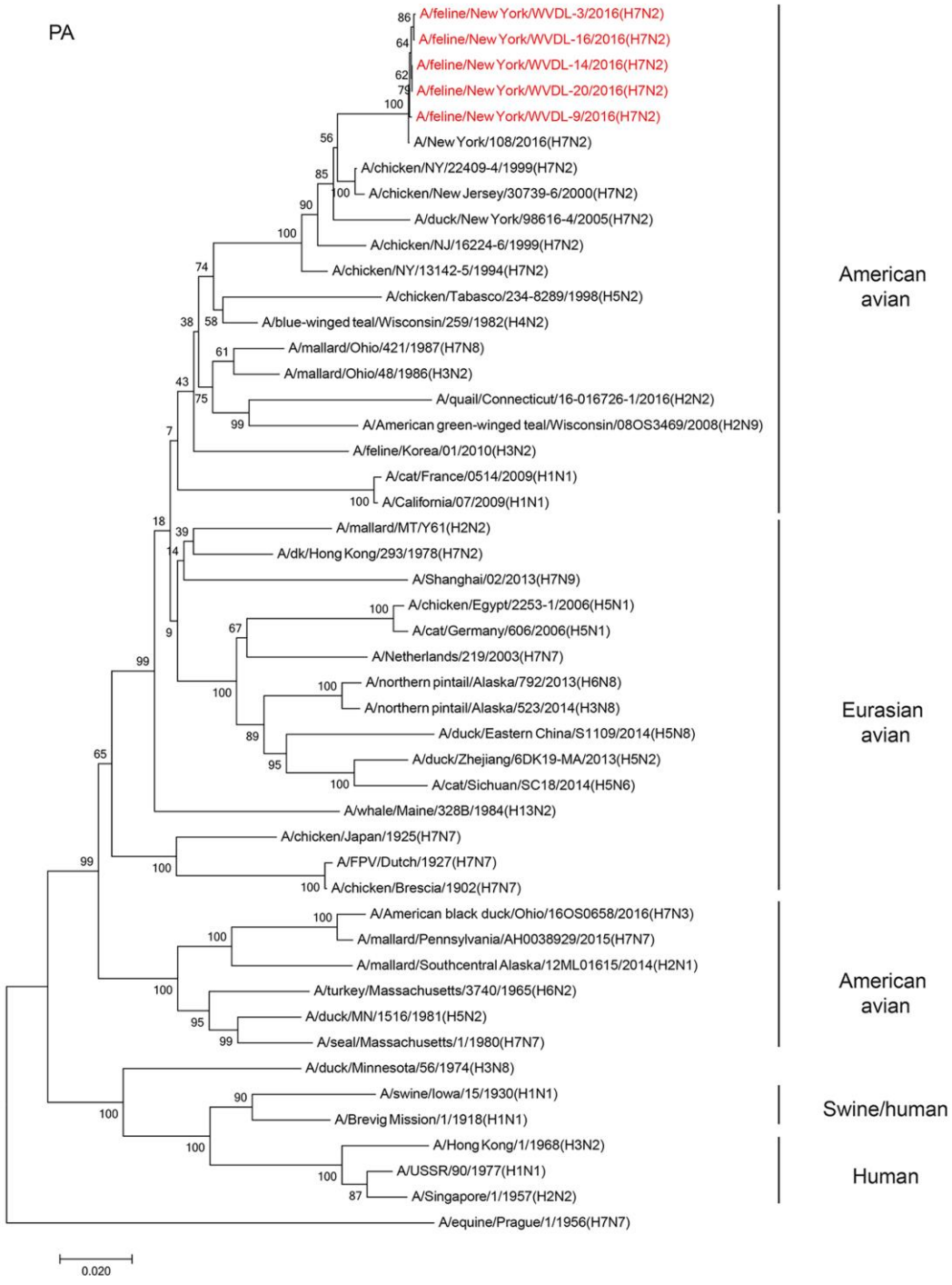

Technical Appendix Figure 5. Phylogenetic tree of influenza A viral PA segments. The optimal tree with the sum of branch length = 1.51709379 is shown. The analysis involved 48 nt sequences. The final dataset contained a total of 2,090 positions.

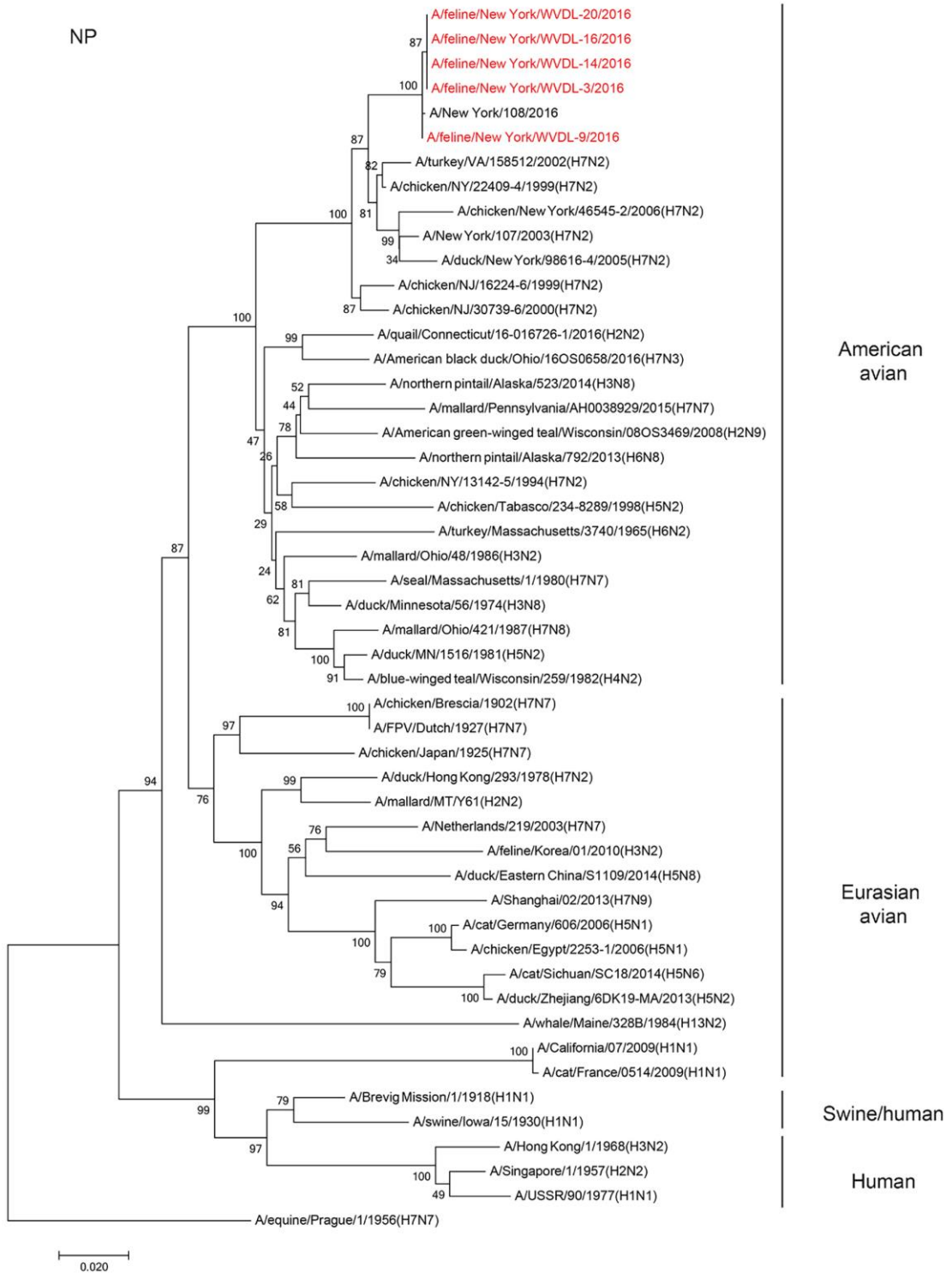

Technical Appendix Figure 6. Phylogenetic tree of influenza A viral NP segments. The optimal tree with the sum of branch length = 1.44906153 is shown. The analysis involved 50 nt sequences. The final dataset contained a total of 1,444 positions.

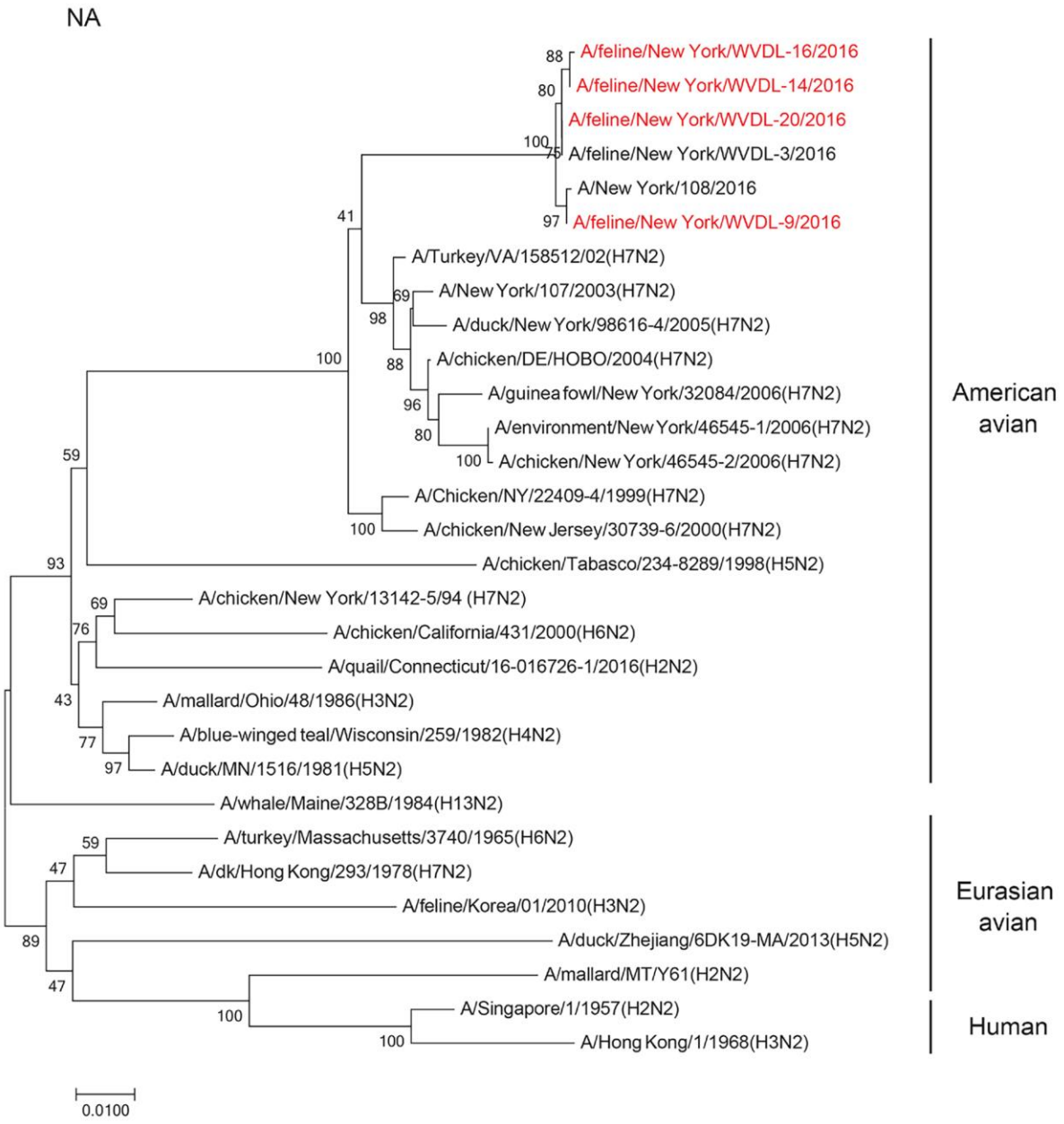

Technical Appendix Figure 7. Phylogenetic tree of influenza A viral NA segments. The optimal tree with the sum of branch length = 0.72173357 is shown. The analysis involved 31 nt sequences. The final dataset contained a total of 1,343 positions.

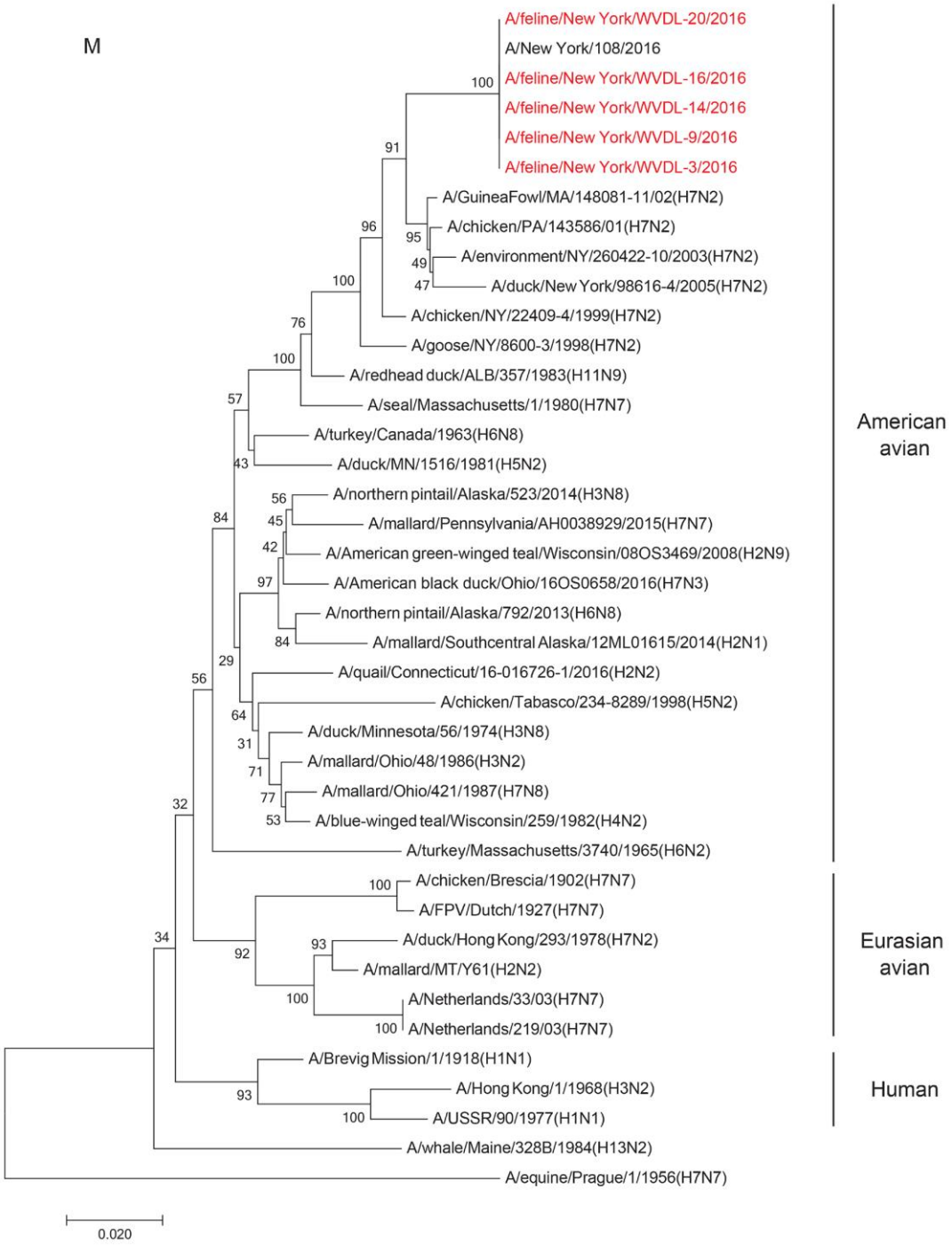

Technical Appendix Figure 8. Phylogenetic tree of influenza A viral M segments. The optimal tree with the sum of branch length = 0.72235656 is shown. The analysis involved 41 nt sequences. The final dataset contained a total of 971 positions.

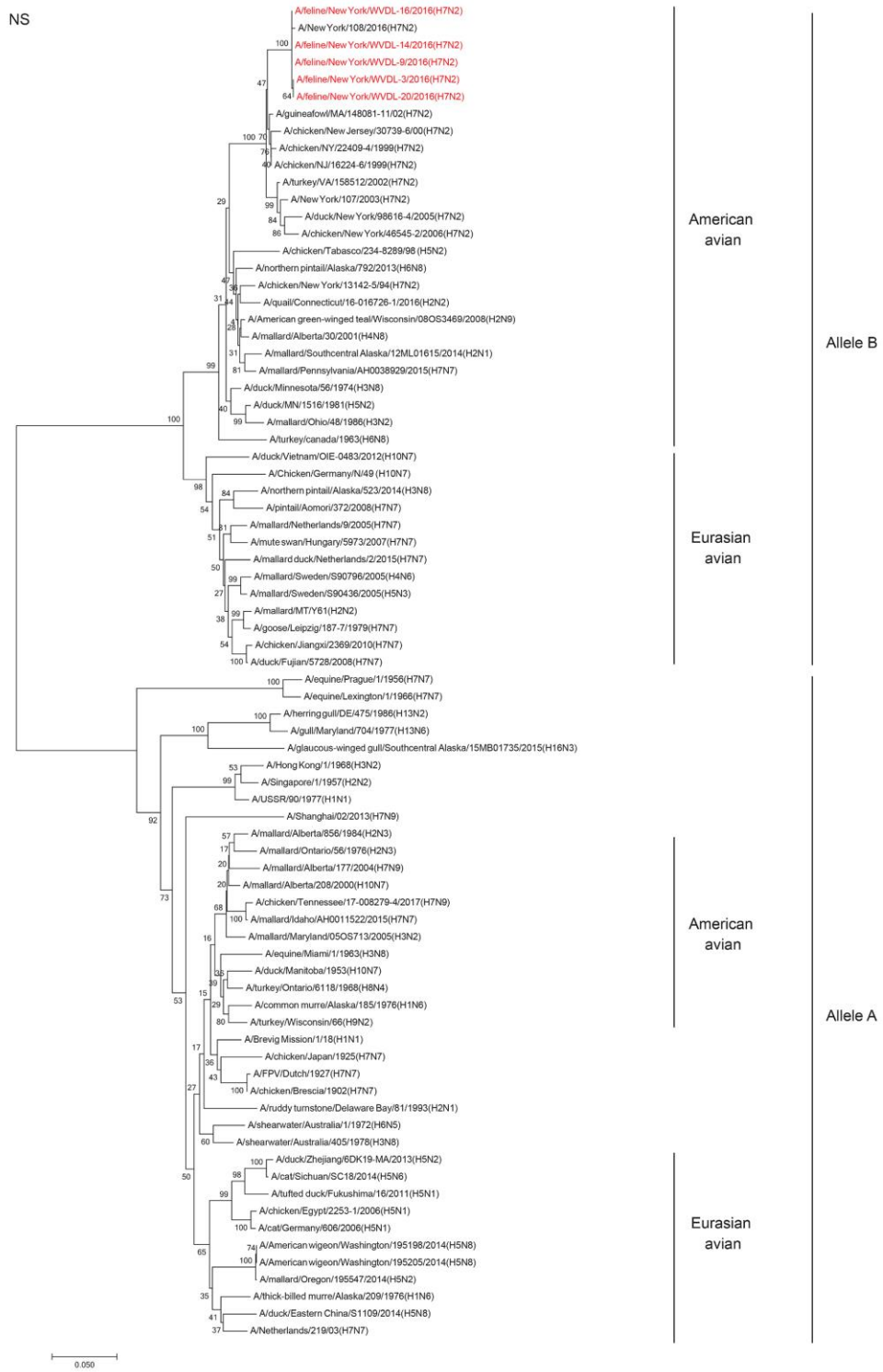

Technical Appendix Figure 9. Phylogenetic tree of influenza A viral NS segments. The optimal tree with the sum of branch length = 1.97636652 is shown. The analysis involved 79 nt sequences. The final dataset contained a total of 811 positions.

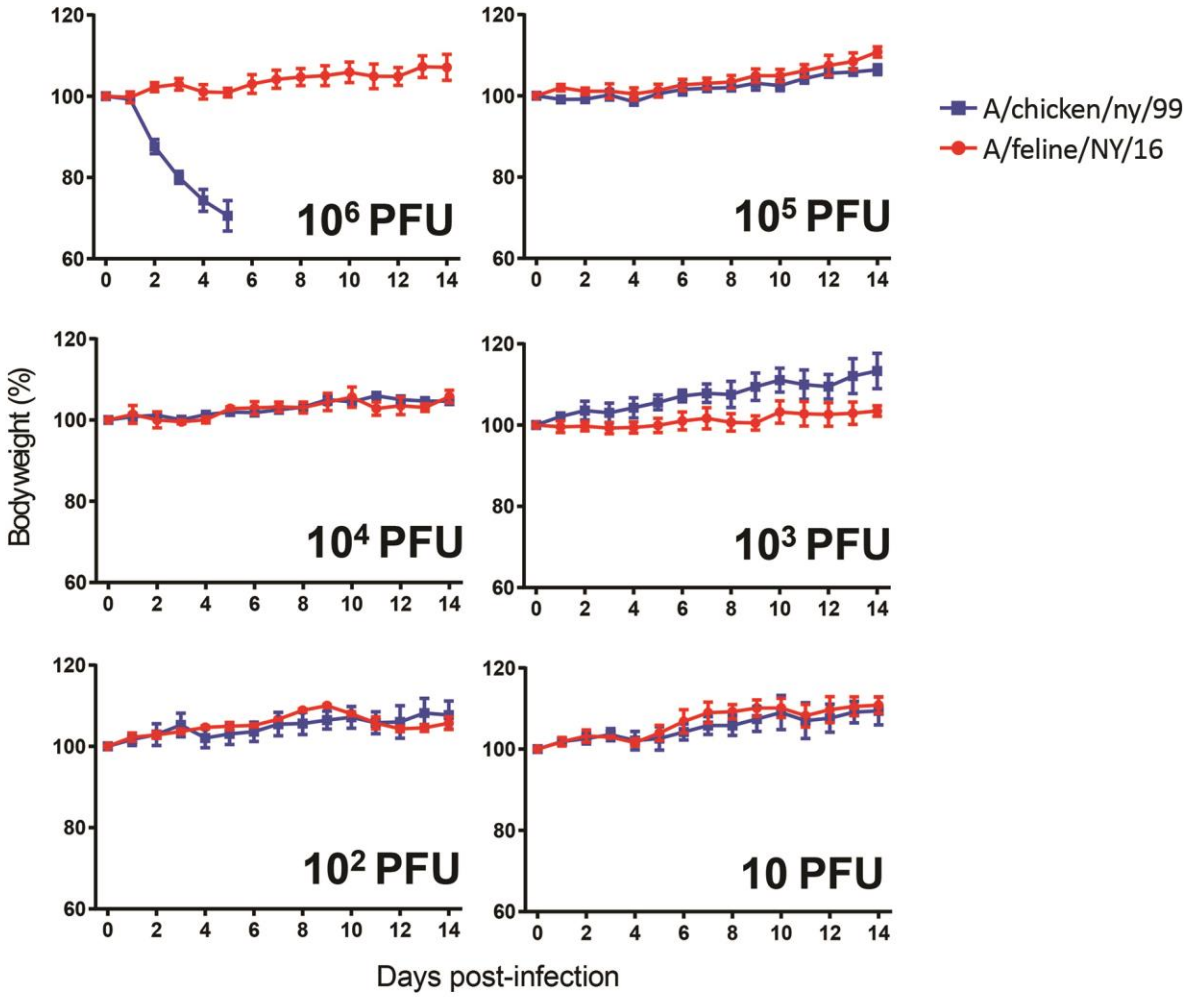

Technical Appendix Figure 10. Pathogenicity of A/feline/NY/16 and A/chicken/NY/99 viruses in mice. Bodyweight changes in mice infected with A/feline/NY/16 and A/chicken/NY/99 viruses. Three mice per group were infected intranasally with A/feline/NY/16 and A/chicken/NY/99 virus in amounts of 10–10^6 PFU. Bodyweight and morbidity and mortality were monitored daily for 14 days.

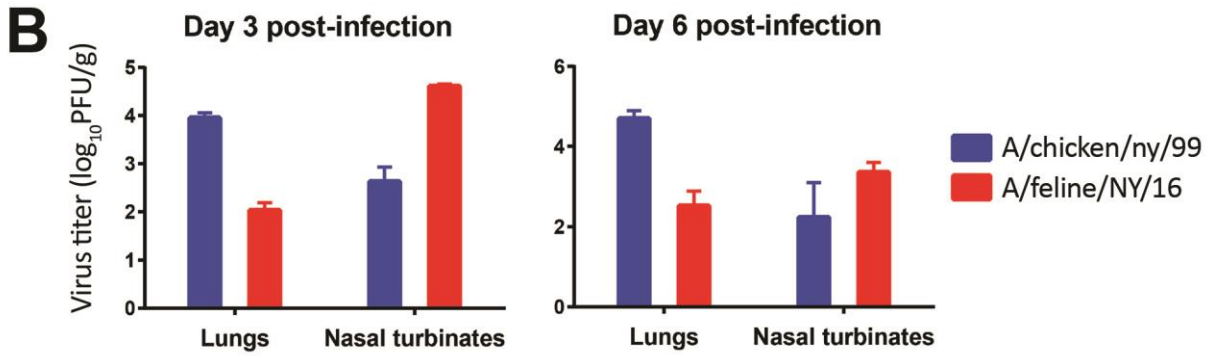

Technical Appendix Figure 11. Virus titers in the organs of infected mice. Six mice per group were infected intranasally with 10^5 PFU of A/feline/NY/16 and A/chicken/NY/99 viruses. Three mice in each group were euthanized on days 3 and 6 postinfection, and organs including brains, lungs, nasal turbinates, kidneys, livers, and spleens were collected. Viruses were isolated only from the lungs and nasal turbinates of infected animals; therefore, the other organs tested are not shown in the figure.

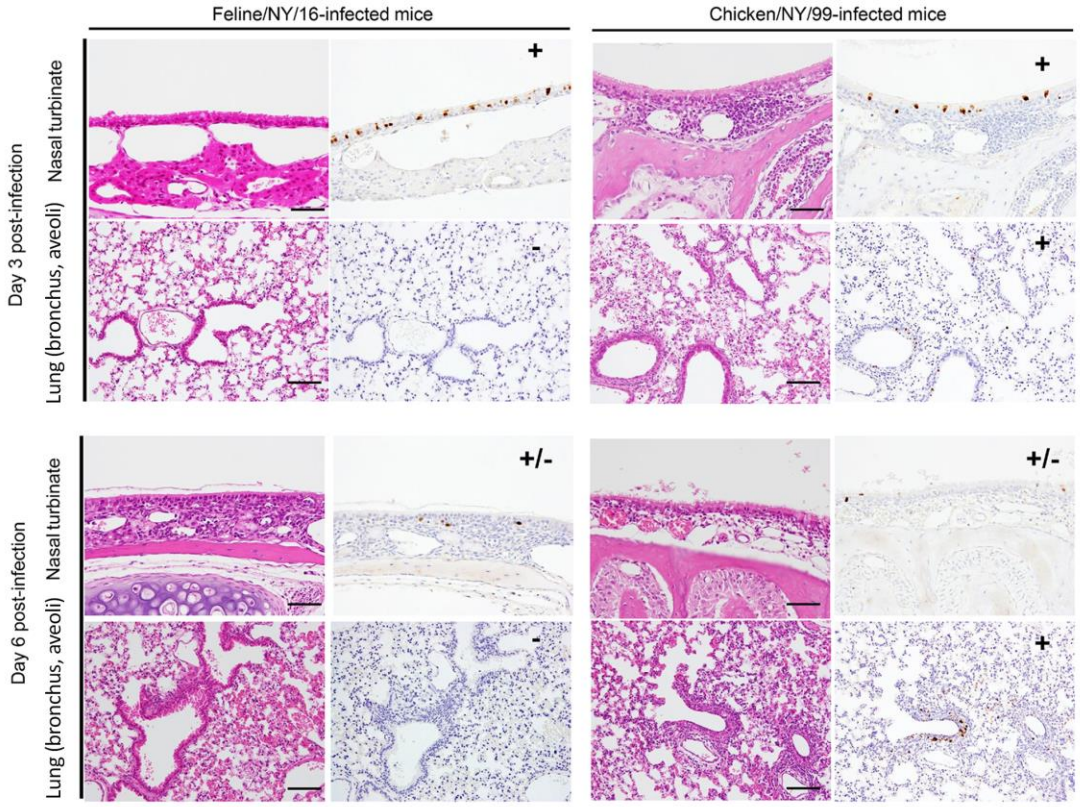

Technical Appendix Figure 12. Immunohistochemical findings in mice infected with A/feline/NY/16 or A/chicken/NY/99 virus. Shown are representative sections of nasal turbinates and lungs of mice infected with the indicated viruses on days 3 and 6 postinfection. Three mice per group were infected intranasally with 10^6 PFU of virus, and tissues were collected on days 3 and 6 post-infection. Influenza virus antigens were detected by a mouse monoclonal antibody for NP. For nasal turbinate sections: -, 0 NP-positive cells; +/–:,NP-positive cells detected in 1 focal region; +, NP-positive cells detected in >3 focal regions. For bronchus and alveolar sections: -, 0 NP-positive cells; +: >6 NP-positive cells. NP-positive cells were detected in focal, but not in diffuse bronchial and alveolar sections. For all analyses, the entire sections were evaluated. Left: H&E staining. Right: immunohistochemical staining for NP. Scale bars, 50 μm (nasal turbinates), 100 μm (lung).

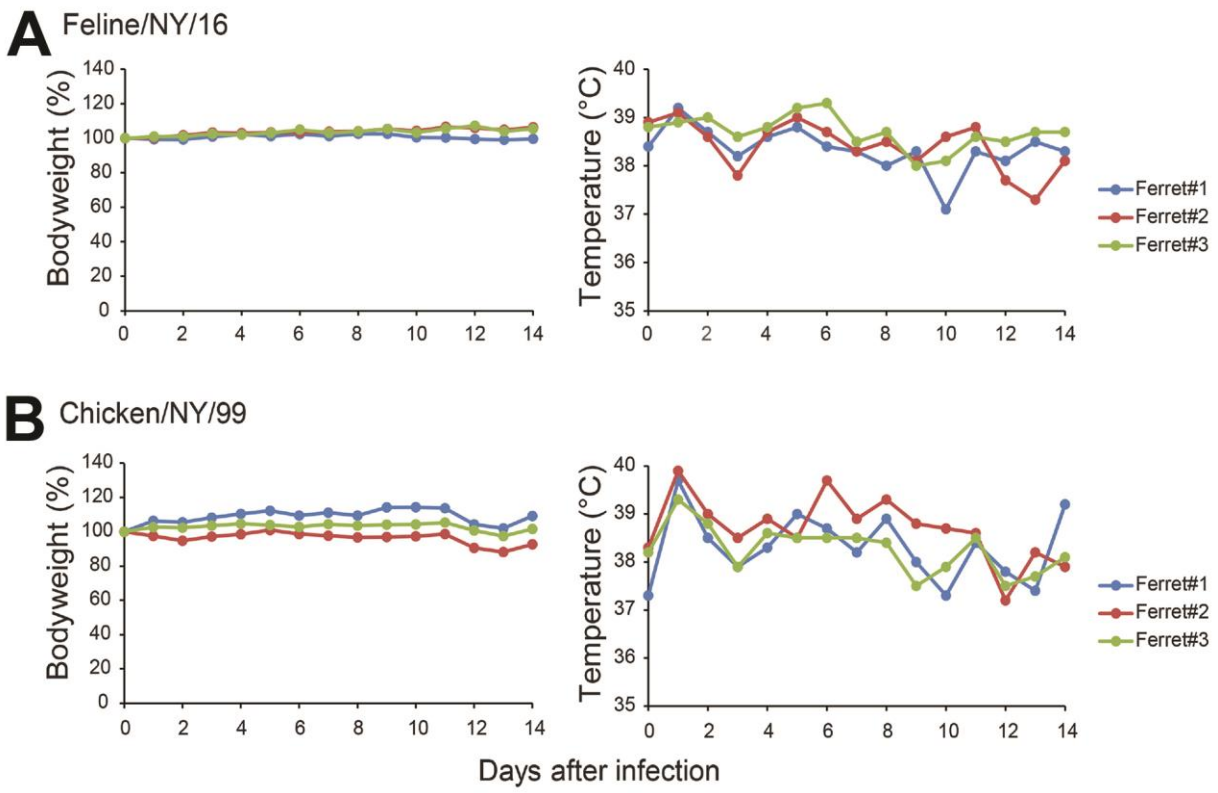

Technical Appendix Figure 13. Bodyweight and temperature changes in ferrets infected with 10^6 PFU of A/feline/NY/16 or A/chicken/NY/99 virus. Bodyweight and temperature were monitored daily for 14 days. A and B) Bodyweight and temperature changes for 3 ferrets per group infected with A/feline/NY/16 virus. C and D) Bodyweight and temperature changes for 3 ferrets per group infected with A/chicken/NY/99 virus.

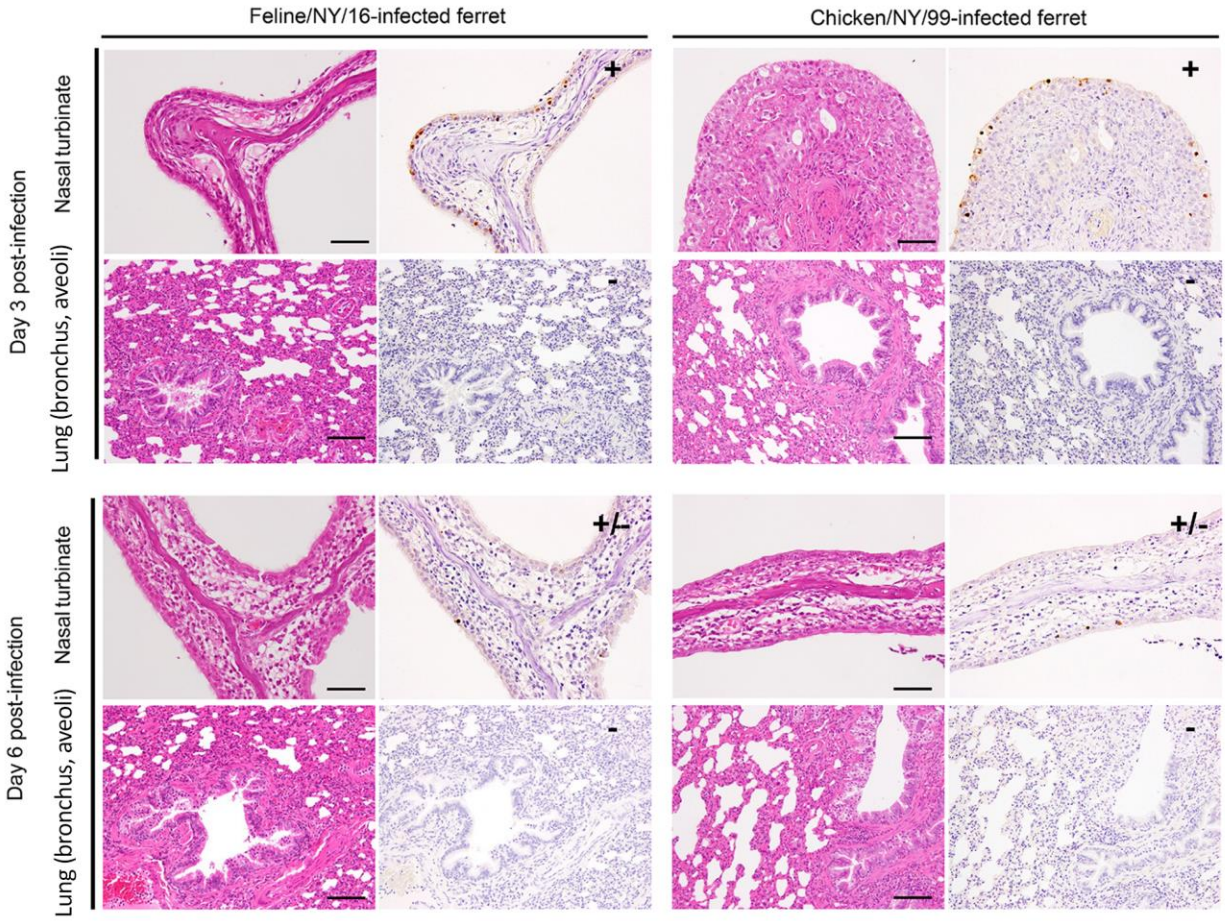

Technical Appendix Figure 14. Immunohistochemical findings in infected ferrets. Shown are representative sections of nasal turbinates and lungs of ferrets infected with the indicated viruses on days 3 and 6 postinfection. Three ferrets per group were infected intranasally with 10^6 PFU of virus, and tissues were collected on days 3 and 6 postinfection. Influenza virus nucleoprotein was detected by a rabbit polyclonal antibody to this protein. For nasal turbinate sections: -, 0 NP-positive cells; +/–:,NP-positive cells detected in 1 focal region; +, NP-positive cells detected in >3 focal regions. For bronchus and alveolar sections: -, 0 NP-positive cells. For all analyses, the entire sections were evaluated. Left: H&E staining. Right: immunohistochemical staining for NP. Scale bars, 50 μm (nasal turbinates), 100 μm (lung).